

Large-scale nuclear structure calculations for spin-dependent WIMP scattering with chiral effective field theory currents

P. Klos,^{1,2,*} J. Menéndez,^{1,2,†} D. Gazit,^{3,‡} and A. Schwenk^{2,1,§}

¹*Institut für Kernphysik, Technische Universität Darmstadt, 64289 Darmstadt, Germany*

²*ExtreMe Matter Institute EMMI, GSI Helmholtzzentrum für Schwerionenforschung GmbH, 64291 Darmstadt, Germany*

³*Racah Institute of Physics and The Hebrew University Center for Nanoscience and Nanotechnology, The Hebrew University, 91904 Jerusalem, Israel*

We perform state-of-the-art large-scale shell-model calculations of the structure factors for elastic spin-dependent WIMP scattering off $^{129,131}\text{Xe}$, ^{127}I , ^{73}Ge , ^{19}F , ^{23}Na , ^{27}Al , and ^{29}Si . This comprehensive survey covers the nonzero-spin nuclei relevant to direct dark matter detection. We include a pedagogical presentation of the formalism necessary to describe elastic and inelastic WIMP-nucleus scattering. The valence spaces and nuclear interactions employed have been previously used in nuclear structure calculations for these mass regions and yield a good spectroscopic description of these isotopes. We use spin-dependent WIMP-nucleus currents based on chiral effective field theory (EFT) at the one-body level and including the leading long-range two-body currents due to pion exchange, which are predicted in chiral EFT. Results for all structure factors are provided with theoretical error bands due to the nuclear uncertainties of WIMP currents in nuclei.

PACS numbers: 95.35.+d, 12.39.Fe, 21.60.Cs

I. INTRODUCTION

About 25% of the energy density of our Universe consists of dark matter, a form of matter that rarely interacts with baryons and has eluded direct observation so far [1, 2]. This large-scale problem is closely connected to new physics at the smallest scales, because dark matter candidates arise naturally in extensions of the Standard Model of particle physics [3]. Prominent dark matter candidates are weakly interacting massive particles (WIMPs). They are predicted in supersymmetric models, as the lightest supersymmetric particles (typically neutralinos) and also in other Standard Model extensions like models with extra dimensions. WIMPs are especially promising candidates, because they account naturally for the dark matter energy density established by observations [2]. Moreover, WIMPs interact with quarks, and thus with baryonic matter, opening the door to direct dark matter detection via elastic scattering off nuclei [4]. Inferring properties of dark matter from direct detection therefore requires detailed knowledge of the structure factors for WIMP scattering off strongly interacting nuclei.

In this work, we focus on spin-dependent (SD) WIMP scattering [5], which is relevant because WIMPs can carry spin. In particular we assume spin 1/2 WIMPs, such as neutralinos or other Majorana fermions. The detection of elastic SD WIMP scattering has been the goal of several past and ongoing experiments [6–12], using different nonzero-spin nuclei as target, but so far without evidence. Evaluating the response of nuclei to WIMPs is challenging. First, it requires matching the WIMP-quark cou-

plings in a particular supersymmetric model to WIMP-nucleon currents. Because quantum chromodynamics (QCD) is nonperturbative at low energies, this is best achieved using effective theories [13–16], in which spin-independent and SD interactions generally enter in leading order. Second, the WIMP-nucleus response requires reliable nuclear-structure calculations. This is especially important for SD interactions, because the response depends on how the spin of the nucleus is distributed among nucleons (due to attractive interactions most of the nucleons pair to spin zero). For the isotopes of interest [6–12], this involves medium-mass to heavier nuclei and is a challenging many-body problem. Previous calculations of SD WIMP scattering off nuclei [5, 17–23] have relied on phenomenological WIMP-nucleon currents, and are based on nuclear-structure calculations that can be improved with recent advances in nuclear interactions and computing capabilities. This work presents progress on these fronts.

The typical momentum transfers involved in WIMP scattering off nuclei are low and of order of the pion mass. In addition, the typical momenta involved in low-energy nuclear structure are similar. At these momentum scales, chiral EFT provides a systematic expansion in powers of momenta Q for nuclear forces and for the coupling to external probes, based on the symmetries of QCD [24, 25]. In addition to the coupling through one-body (1b) currents, generally at leading order, two-body (2b) currents enter at higher order and are quantitatively important.

In previous work [15] we have derived the currents for SD WIMP scattering off nuclei based on chiral EFT, including 1b currents and the leading long-range 2b currents due to pion exchange, which are predicted in chiral EFT. As an application, we focused on the scattering off $^{129,131}\text{Xe}$, as they provide the most stringent limits for WIMP coupling to neutrons [26]. Our results have recently been adopted as benchmark for the XENON100

* E-mail: pklos@theorie.ikp.physik.tu-darmstadt.de

† E-mail: javier.menendez@physik.tu-darmstadt.de

‡ E-mail: doron.gazit@mail.huji.ac.il

§ E-mail: schwenk@physik.tu-darmstadt.de

SD WIMP-nucleon cross-section limits [12], and have also been used in Ref. [27].

More generally, two-body contributions to weak neutral currents have been shown to be key for providing accurate predictions of neutrino-deuteron scattering at solar neutrino energies for SNO [28, 29]. Weak neutral currents based on chiral EFT have been explored for light nuclei and neutrino breakup in core-collapse supernovae [30–33], and 2b weak charged currents have been shown to provide important contributions to Gamow-Teller transitions and double-beta decays of medium-mass nuclei [34]. Following our previous work [15], Refs. [35, 36] have reported simple prescriptions to approximately include the effects of chiral 2b currents in previous calculations of SD WIMP-nucleus scattering.

This work expands Ref. [15] by presenting state-of-the-art large-scale shell-model calculations that describe the nonzero-spin states of all isotopes that are experimentally relevant for SD WIMP direct detection: $^{129,131}\text{Xe}$, ^{127}I , ^{73}Ge , ^{19}F , ^{23}Na , ^{27}Al , and ^{29}Si . The nuclear-structure calculations are performed with interactions and valence spaces that have been tested in these mass regions. Based on the calculated ground states, we predict the structure factors for elastic SD WIMP scattering, including chiral 1b and 2b currents with an improved treatment of the momentum-transfer dependence for higher momentum transfers. We provide theoretical error bands due to the uncertainties of WIMP currents in nuclei.

The outline of this article is as follows. In Sec. II, we derive the WIMP currents in nuclei based on chiral EFT. All microscopic inputs needed to compute the structure factors of SD WIMP-nucleus scattering are discussed in Sec. III. Combined with detailed Appendixes, this includes a pedagogical presentation of the formalism necessary to describe elastic and inelastic WIMP-nucleus scattering. In Sec. IV, we present large-scale nuclear-structure calculations that describe the nuclei relevant for SD WIMP direct detection, and compare our results to experiment. We then calculate the structure factors for elastic SD WIMP scattering for all cases using chiral EFT currents. We discuss in detail the role of 2b currents and their uncertainties; the contributions of different multipole operators to the total response; and the issue of proton/neutron versus isoscalar/isovector decompositions of the structure factors. Finally, we summarize in Sec. V and give an outlook for future improvements of the nuclear physics of dark matter detection.

II. WIMP-NUCLEUS INTERACTIONS

A. Chiral EFT and WIMP currents

At the WIMP-quark level, the low-momentum-transfer Lagrangian density \mathcal{L} for SD interactions is taken to be

an axial-vector-axial-vector coupling [5, 37]:

$$\begin{aligned} \mathcal{L}_\chi^{\text{SD}} &= \frac{G_F}{\sqrt{2}} \int d^3\mathbf{r} j^\mu(\mathbf{r}) J_\mu^A(\mathbf{r}) \\ &= -\frac{G_F}{\sqrt{2}} \int d^3\mathbf{r} \bar{\chi} \boldsymbol{\gamma} \boldsymbol{\gamma}_5 \chi \cdot \sum_q A_q \bar{\psi}_q \boldsymbol{\gamma} \boldsymbol{\gamma}_5 \psi_q, \end{aligned} \quad (1)$$

where G_F is the Fermi coupling constant, and $J_\mu^A(\mathbf{r})$ and $j^\mu(\mathbf{r})$ denote the hadronic current and the leptonic current of the WIMP, respectively. χ is the neutralino field, ψ_q are the fields of $q = u, d, s$ quarks, and A_q the neutralino-quark coupling constants. The temporal components can be neglected, because the velocities of WIMPs are expected to be nonrelativistic with $v/c \sim 10^{-3}$. We also neglect contributions to the Lagrangian density other than axial-vector currents, such as polar-vector currents, which are suppressed by the momentum transfer over the nucleon mass p/m [5]. This approximation will be studied in a future paper.

For the WIMP-nucleus response, the SD WIMP interaction couples dominantly to a single nucleon, but also to pairs of nucleons. At the one-nucleon level, the quark currents are replaced by their expectation value in the nucleon, leading to 1b axial-vector currents $\mathbf{J}_{i,1b}$. In the nucleus, the currents are summed over all A nucleons:

$$\sum_q A_q \bar{\psi}_q \boldsymbol{\gamma} \boldsymbol{\gamma}_5 \psi_q \longrightarrow \sum_{i=1}^A \mathbf{J}_{i,1b} = \sum_{i=1}^A (\mathbf{J}_{i,1b}^0 + \mathbf{J}_{i,1b}^3), \quad (2)$$

with the isoscalar $\mathbf{J}_{i,1b}^0$ and isovector $\mathbf{J}_{i,1b}^3$ parts.

The coupling of the isoscalar part is given by [5]

$$a_0 = (A_u + A_d)(\Delta u + \Delta d) + 2A_s \Delta s, \quad (3)$$

where $\Delta u, \Delta d, \Delta s$ are defined as $\bar{\psi}_q \boldsymbol{\gamma} \boldsymbol{\gamma}_5 \psi_q = \Delta q \boldsymbol{\sigma} / 2$, with the nucleon spin $\boldsymbol{\sigma} / 2$. Therefore, $\mathbf{J}_{i,1b}^0 = a_0 \boldsymbol{\sigma} / 2$, and a_0 receives contributions from the isoscalar combination of the u and d quarks to the spin of the nucleon, as well as from the s quark. Analogously, the isovector coupling can be written as

$$a_1 = (A_u - A_d)(\Delta u - \Delta d) = (A_u - A_d)g_A, \quad (4)$$

where g_A is the axial coupling constant. This shows that the isovector part $\mathbf{J}_{i,1b}^3$ of the axial-vector WIMP-nucleon coupling is identical, up to replacing a_1 by g_A , to the axial-vector part of the weak neutral current.

B. Coupling to one nucleon

The weak neutral current was derived within chiral EFT for calculations of low-energy electroweak reactions. At lowest orders Q^0 and Q^2 , there are only 1b currents. For the isovector part of the axial-vector WIMP-nucleon current, this leads to [15]

$$\mathbf{J}_{i,1b}^3 = \frac{1}{2} a_1 \tau_i^3 \left(\frac{g_A(p^2)}{g_A} \boldsymbol{\sigma}_i - \frac{g_P(p^2)}{2m g_A} (\mathbf{p} \cdot \boldsymbol{\sigma}_i) \mathbf{p} \right), \quad (5)$$

where τ_i^3 denotes the isospin, $\mathbf{p} = \mathbf{p}_i - \mathbf{p}'_i$ the momentum transfer from nucleons to neutralinos, and $g_A(p^2)$ and $g_P(p^2)$ the axial and pseudo-scalar couplings. The momentum transfer dependence of $g_A(p^2)$ and $g_P(p^2)$ is due to loop corrections and pion propagators. To order Q^2 , one has [38]

$$\frac{g_A(p^2)}{g_A} = 1 - 2 \frac{p^2}{\Lambda_A^2}, \quad (6)$$

$$g_P(p^2) = \frac{2g_{\pi pn}F_\pi}{m_\pi^2 + p^2} - 4 \frac{mg_A}{\Lambda_A^2}, \quad (7)$$

with $\Lambda_A = 1040$ MeV, pion mass $m_\pi = 138.04$ MeV, pion decay constant $F_\pi = 92.4$ MeV, and $g_{\pi pn} = 13.05$. Chiral 1b currents are similar to the currents used in previous calculations of WIMP scattering off nuclei [5]. The differences are that the $1/\Lambda_A^2$ terms were neglected and the Goldberger-Treiman relation was implicitly used to write $\frac{g_P(p^2)}{2mg_A} \approx \frac{1}{m_\pi^2 + p^2}$. Both present few percent corrections, but the former increases with momentum transfer.

The axial-vector part of the weak neutral currents is isovector in the Standard Model, neglecting the strange quark contribution to a_0 in Eq. (3). Therefore, higher-order Q^2 contributions to the isoscalar WIMP-nucleon current $\mathbf{J}_{i,1b}^0 = a_0 \boldsymbol{\sigma}/2$ depend on models of currents in the nucleon. To order Q^2 , these lead to 1b currents with a form-factor mass-scale $\sim \Lambda_A$ [39] and without pion propagator contributions. Because the isovector $1/\Lambda_A^2$ terms contribute at the few percent level for the typical momentum transfers in WIMP scattering, we chose to neglect higher-order isoscalar current contributions, as opposed to introducing a model dependence at this level.

C. Coupling to two nucleons

At order Q^3 , 2b currents enter in chiral EFT [40]. We consider their long-range parts due to pion exchange,

which are predicted in chiral EFT, and for medium-mass nuclei were found to dominate over the short-range parts [15]. Because of their pion-exchange nature, the axial-vector part of the weak neutral 2b current is isovector, $\mathbf{J}_{2b} = \sum_{i<j}^A \mathbf{J}_{ij}^3$, with

$$\begin{aligned} \mathbf{J}_{12}^3 = & -\frac{g_A}{2F_\pi^2} (\tau_1 \times \tau_2)^3 \left(\frac{\boldsymbol{\sigma}_2 \cdot \mathbf{k}_2}{m_\pi^2 + k_2^2} \left[\left(c_4 + \frac{1}{4m} \right) (\boldsymbol{\sigma}_1 \times \mathbf{k}_2) \right. \right. \\ & \left. \left. + i \frac{\mathbf{p}_1 + \mathbf{p}'_1}{4m} + \left(\frac{1 + \hat{c}_6}{4m} \right) (\boldsymbol{\sigma}_1 \times \mathbf{q}) \right] - (1 \leftrightarrow 2) \right) \\ & - \frac{g_A}{F_\pi^2} c_3 \left[\tau_1^3 \frac{(\boldsymbol{\sigma}_1 \cdot \mathbf{k}_1) \mathbf{k}_1}{m_\pi^2 + k_1^2} + \tau_2^3 \frac{(\boldsymbol{\sigma}_2 \cdot \mathbf{k}_2) \mathbf{k}_2}{m_\pi^2 + k_2^2} \right], \quad (8) \end{aligned}$$

where $\mathbf{k}_i = \mathbf{p}'_i - \mathbf{p}_i$ and $\mathbf{q} = -\mathbf{k}_1 - \mathbf{k}_2$. This improves the treatment of the momentum-transfer dependence compared to our previous work [15], as it does not make the approximation of low-momentum transfers in the currents [40]. As a result, two momentum transfers appear, \mathbf{k}_1 and \mathbf{k}_2 , and also a new term proportional to $1 + \hat{c}_6$, which vanishes in the limit of zero momentum transfer.

As in Ref. [15], we take into account the normal-ordered one-body part of chiral 2b currents. This is obtained by summing the second nucleon j over occupied states in a spin and isospin symmetric reference state or core, which we take as a Fermi gas: $\mathbf{J}_{i,2b}^{\text{eff}} = \sum_j (1 - P_{ij}) \mathbf{J}_{ij}^3$. The exchange operator P_{ij} includes all two-body exchange contributions. Normal ordering is expected to be a very good approximation for medium-mass and heavy nuclei, because of phase-space restrictions of normal Fermi systems at low energies [41].

The resulting effective 2b currents $\mathbf{J}_{i,2b}^{\text{eff}}$ are derived in detail in Appendix A. We find that the leading long-range 2b currents lead to three different contributions. First, there is a renormalization of the axial coupling [15],

$$\begin{aligned} \mathbf{J}_{i,2b}^{\text{eff},\sigma}(\rho, \mathbf{p}, \mathbf{P}) = & -g_A \boldsymbol{\sigma}_i \frac{\tau_i^3}{2} \frac{\rho}{2F_\pi^2} \left(\frac{1}{3} \left(-c_3 + \frac{1}{4m} \right) \left[I_1^\sigma(\rho, |\mathbf{P} - \mathbf{p}|) + I_1^\sigma(\rho, |\mathbf{P} + \mathbf{p}|) \right] \right. \\ & + \frac{1}{3} \left(c_4 + \frac{1}{4m} \right) \left[3I_2^\sigma(\rho, |\mathbf{P} - \mathbf{p}|) - I_1^\sigma(|\mathbf{P} - \mathbf{p}|) + 3I_2^\sigma(\rho, |\mathbf{P} + \mathbf{p}|) - I_1^\sigma(|\mathbf{P} + \mathbf{p}|) \right] \\ & \left. + \left(\frac{1 + \hat{c}_6}{12m} \right) \left[I_{c_6}(\rho, |\mathbf{P} - \mathbf{p}|) \frac{\mathbf{p} \cdot (\mathbf{P} - \mathbf{p})}{(\mathbf{P} - \mathbf{p})^2} - I_{c_6}(\rho, |\mathbf{P} + \mathbf{p}|) \frac{\mathbf{p} \cdot (\mathbf{P} + \mathbf{p})}{(\mathbf{P} + \mathbf{p})^2} \right] \right), \quad (9) \end{aligned}$$

which depends on the density ρ , the momentum transfer \mathbf{p} and the total momentum $\mathbf{P} = \mathbf{p}_i + \mathbf{p}'_i$ (due to the exchange terms). Such renormalization was also found considering chiral three-nucleon forces as density-dependent two-body interactions [42]. Second, there is a contribution to the pseudo-scalar coupling,

$$\begin{aligned} \mathbf{J}_{i,2b}^{\text{eff},P}(\rho, \mathbf{p}, \mathbf{P}) = & -g_A \frac{\tau_i^3}{2} (\mathbf{p} \cdot \boldsymbol{\sigma}_i) \mathbf{p} \frac{\rho}{2F_\pi^2} \left(\frac{4c_3}{m_\pi^2 + p^2} - \frac{1}{3} (c_3 + c_4) \frac{I^P(\rho, |\mathbf{P} - \mathbf{p}|) + I^P(\rho, |\mathbf{P} + \mathbf{p}|)}{p^2} \right. \\ & \left. + \left(\frac{1 + \hat{c}_6}{12m} \right) \left[\frac{I_{c_6}(\rho, |\mathbf{P} - \mathbf{p}|)}{(\mathbf{P} - \mathbf{p})^2} + \frac{I_{c_6}(\rho, |\mathbf{P} + \mathbf{p}|)}{(\mathbf{P} + \mathbf{p})^2} \right] \right), \quad (10) \end{aligned}$$

and third, chiral 2b currents induce pseudo-scalar-type currents depending on the total momentum,

$$\mathbf{J}_{i,2b}^{\text{eff},P1}(\rho, \mathbf{p}, \mathbf{P}) \sim g_A \frac{\tau_i^3}{2} (\mathbf{p} \cdot \boldsymbol{\sigma}_i) \mathbf{P}, \quad (11)$$

$$\mathbf{J}_{i,2b}^{\text{eff},P2}(\rho, \mathbf{p}, \mathbf{P}) \sim g_A \frac{\tau_i^3}{2} (\mathbf{P} \cdot \boldsymbol{\sigma}_i) \mathbf{p}, \quad (12)$$

$$\mathbf{J}_{i,2b}^{\text{eff},P3}(\rho, \mathbf{p}, \mathbf{P}) \sim g_A \frac{\tau_i^3}{2} (\mathbf{P} \cdot \boldsymbol{\sigma}_i) \mathbf{P}, \quad (13)$$

whose analytical expressions can be found in Appendix A. The functions $I_1^\sigma(\rho, Q)$, $I_2^\sigma(\rho, Q)$, $I^P(\rho, Q)$, and $I_{c_6}(\rho, Q)$ are given by integrals due to the summation over occupied states in the exchange terms. They can be evaluated analytically, and the explicit expressions are given in Appendix A.

The contributions from 2b currents in Eqs. (9)–(13) depend on the density of the reference state $\rho = 2k_F^3/(3\pi^2)$ (k_F is the Fermi momentum) and on the low-energy couplings c_3 , c_4 , and \hat{c}_6 . For the density ρ we take the range $\rho = 0.10 \dots 0.12 \text{ fm}^{-3}$, appropriate for the nuclei considered (see also Ref. [34]). The low-energy couplings c_3 and c_4 also enter pion-nucleon and nucleon-nucleon interactions and have been determined from data. Here, we consider the c_3, c_4 values from the next-to-next-to-next-to-leading order (N³LO) nucleon-nucleon (NN) potentials of Ref. [43] (EM) and Ref. [44] (EGM), as well as from the NN partial wave analysis (PWA) [45]. To be conservative, we also consider the estimated uncertainty in these values expected from higher-order order contributions, $\delta c_3 = -\delta c_4 \approx 1 \text{ GeV}^{-1}$ [24]. The resulting c_3 and c_4 values are given in Tables I and II. We take $\hat{c}_6 = 5.83$ from Ref. [46].

In Table I, we study the P dependence of the 2b current contribution to the axial coupling, which we write as $\mathbf{J}_{i,2b}^{\text{eff},\sigma}(\rho, P) = -g_A \boldsymbol{\sigma}_i \frac{\tau_i^3}{2} \frac{\rho}{F_\pi^2} J^\sigma(\rho, P)$, at $p = 0$. We compare $J^\sigma(\rho, P)$ for the Fermi gas mean value $P^2 = 6k_F^2/5$ and $P = 0$ at a density $\rho = 0.10 \text{ fm}^{-3}$ and for the dif-

TABLE I. Comparison of $J^\sigma(\rho, P)$, which describes the axial contribution at $p = 0$ from the normal-ordered one-body part of the long-range 2b currents, $\mathbf{J}_{i,2b}^{\text{eff},\sigma}(\rho, P) = -g_A \boldsymbol{\sigma}_i \frac{\tau_i^3}{2} \frac{\rho}{F_\pi^2} J^\sigma(\rho, P)$, evaluated at the Fermi gas mean value $P^2 = 6k_F^2/5$ and at $P = 0$ for a density $\rho = 0.10 \text{ fm}^{-3}$. The variation is shown for all c_3, c_4 sets considered, and the relative variation $\Delta J^\sigma/J^\sigma$ between the Fermi gas mean value and $P = 0$ is given. The c_i and J^σ values are in GeV^{-1} .

	c_3	c_4	$J^\sigma(\rho, P)$	$J^\sigma(\rho, P = 0)$	$\Delta J^\sigma/J^\sigma$
EM	-3.2	5.4	3.20	2.84	0.11
EM+ δc_i	-2.2	4.4	2.57	2.26	0.12
EGM	-3.4	3.4	2.29	2.10	0.08
EGM+ δc_i	-2.4	2.4	1.66	1.53	0.08
PWA	-4.78	3.96	2.78	2.59	0.07
PWA+ δc_i	-3.78	2.96	2.15	2.01	0.06

TABLE II. Values for all c_3, c_4 sets considered of the long-range 2b current contributions $\delta a_i(p = 0)$ (axial) and $\delta a_i^P(p = m_\pi)$ (pseudo-scalar) for the density range $\rho = 0.10 \dots 0.12 \text{ fm}^{-3}$. The c_i values are in GeV^{-1} .

	c_3	c_4	$\delta a_1(p = 0)$	$\delta a_1^P(p = m_\pi)$
EM	-3.2	5.4	-(0.26...0.32)	0.32...0.38
EM+ δc_i	-2.2	4.4	-(0.20...0.25)	0.23...0.27
EGM	-3.4	3.4	-(0.19...0.24)	0.33...0.39
EGM+ δc_i	-2.4	2.4	-(0.14...0.17)	0.24...0.28
PWA	-4.78	3.96	-(0.23...0.29)	0.45...0.54
PWA+ δc_i	-3.78	2.96	-(0.18...0.23)	0.36...0.43

ferent c_3, c_4 sets considered. Table I shows that the P dependence is very weak: $J^\sigma(\rho, 0)$ varies by less than 12% over the relevant P range. For other densities in the range $\rho = 0.10 \dots 0.12 \text{ fm}^{-3}$ this variation is even smaller. Because 2b currents are a correction to the leading 1b currents, we therefore set $P = 0$ in the axial 2b current contribution, Eq. (9). As the contributions from Eqs. (11)–(13) are expected to be weaker, we therefore consistently set $P = 0$, so that only the standard pseudo-scalar part, Eq. (10), contributes. Finally to connect to our previous work, for $p = P = 0$, both I_1^σ and I_2^σ lead to [15]

$$\begin{aligned} I^\sigma(\rho, p = P = 0) &\equiv I_1^\sigma(\rho, p = P = 0) = I_2^\sigma(\rho, p = P = 0) \\ &= 1 - \frac{3m_\pi^2}{k_F^2} + \frac{3m_\pi^3}{k_F^3} \arctan\left(\frac{k_F}{m_\pi}\right), \end{aligned} \quad (14)$$

where $I^\sigma(\rho, p = P = 0) = 0.58 \dots 0.60$ depends only weakly on the density in the range $\rho = 0.10 \dots 0.12 \text{ fm}^{-3}$.

For $P = 0$, the 2b current contribution to the axial part, Eq. (9), can be written as a momentum- and density-dependent renormalization $\delta a_1(p)$,

$$\mathbf{J}_{i,2b}^{\text{eff},\sigma} = g_A \boldsymbol{\sigma}_i \frac{\tau_i^3}{2} \delta a_1(p), \quad (15)$$

with

$$\begin{aligned} \delta a_1(p) &= -\frac{\rho}{F_\pi^2} \left[\frac{1}{3} \left(c_4 + \frac{1}{4m} \right) \left[3I_2^\sigma(\rho, p) - I_1^\sigma(\rho, p) \right] \right. \\ &\quad \left. + \frac{1}{3} \left(-c_3 + \frac{1}{4m} \right) I_1^\sigma(\rho, p) - \left(\frac{1 + \hat{c}_6}{12m} \right) I_{c_6}(\rho, p) \right]. \end{aligned} \quad (16)$$

Similarly, we write the 2b-current contribution to the pseudo-scalar coupling, Eq. (10), as a momentum- and density-dependent renormalization $\delta a_1^P(p)$,

$$\mathbf{J}_{i,2b}^{\text{eff},P} = g_A \frac{\tau_i^3}{2} (\mathbf{p} \cdot \boldsymbol{\sigma}_i) \mathbf{p} \frac{\delta a_1^P(p)}{p^2}, \quad (17)$$

with

$$\delta a_1^P(p) = \frac{\rho}{F_\pi^2} \left[\frac{-2c_3 p^2}{m_\pi^2 + p^2} + \frac{c_3 + c_4}{3} I^P(\rho, p) - \frac{1 + \hat{c}_6}{12m} I_{c_6}(\rho, p) \right]. \quad (18)$$

The ranges of $\delta a_1(p)$ and $\delta a_1^P(p)$ are given in Table II for the c_3, c_4 values and the density range considered. We find that $\delta a_1(p)$ reduces the axial part of the current by 14%...32% at $p = 0$. The momentum transfer dependence is mild, as the reduction is 16%...36% at $p = m_\pi$. Moreover, $\delta a_1^P(p)$ increases the pseudo-scalar part of the current by 23%...54% at $p = m_\pi$. At lower momentum transfers this enhancement is weaker, while it is more significant for higher p . These results are consistent with studies of Gamow-Teller transitions and double-beta decays [34]. As discussed in Ref. [15], in addition to the long-range 2b pion-exchange currents, there are short-range 2b currents for the isoscalar and isovector parts, which are included as contact terms in chiral EFT. The isovector short-range 2b parts only lead to small contributions [34]. Therefore, we neglect short-range 2b currents at this level, which is also consistent with neglecting higher-order (short-range) 1b isoscalar currents, see Sec. II B.

D. Combined response

Combining the 1b and the long-range 2b currents to order Q^3 in chiral EFT (replacing g_A by a_1 for the latter), the isovector part of the axial-vector WIMP current at the normal-ordered one-body level is given by [15]

$$\mathbf{J}_{i,1b+2b}^3 = \frac{1}{2} a_1 \tau_i^3 \left[\left(\frac{g_A(p^2)}{g_A} + \delta a_1(p) \right) \boldsymbol{\sigma}_i + \left(-\frac{g_P(p^2)}{2m g_A} + \frac{\delta a_1^P(p)}{p^2} \right) (\mathbf{p} \cdot \boldsymbol{\sigma}_i) \mathbf{p} \right]. \quad (19)$$

III. WIMP-NUCLEUS SCATTERING AND STRUCTURE FACTORS

A. WIMP-nucleus scattering

The differential cross section for SD WIMP elastic scattering off a nucleus in the initial state $|i\rangle$ to the final state $|f\rangle$ can be obtained from the low-momentum-transfer Lagrangian density of Eq. (1). A detailed derivation is performed in Appendix B. The final result is [5]

$$\begin{aligned} \frac{d\sigma}{dp^2} &= \frac{2}{(2J_i + 1)\pi v^2} \sum_{s_f, s_i} \sum_{M_f, M_i} |\langle f | \mathcal{L}_\chi^{\text{SD}} | i \rangle|^2 \\ &= \frac{8G_F^2}{(2J_i + 1)v^2} S_A(p), \end{aligned} \quad (20)$$

where the sum $s_f, s_i = \pm 1/2$ is over neutralino spin projections, and the sum M_f, M_i is over the projections of the total angular momentum of the final and initial states J_f, J_i , respectively; v is the WIMP velocity, and $S_A(p)$ the axial-vector structure factor. The structure factor can be decomposed as a sum over multipoles L with reduced matrix elements of the longitudinal \mathcal{L}_L^5 , transverse electric $\mathcal{T}_L^{\text{el}5}$, and transverse magnetic $\mathcal{T}_L^{\text{mag}5}$ projections of the axial-vector currents:

$$S_A(p) = \sum_{L \geq 0} |\langle J_f | \mathcal{L}_L^5 | J_i \rangle|^2 + \sum_{L \geq 1} \left(|\langle J_f | \mathcal{T}_L^{\text{el}5} | J_i \rangle|^2 + |\langle J_f | \mathcal{T}_L^{\text{mag}5} | J_i \rangle|^2 \right). \quad (21)$$

The multipole contributions are obtained from the WIMP-nucleus currents $\mathbf{J}^A(\mathbf{r})$. At the effective one-body level, chiral 1b and 2b currents lead to (see Appendix B for the definition of the multipole operators and details of the derivation)

$$\begin{aligned} \mathcal{L}_L^5(p) &= \frac{i}{\sqrt{2L+1}} \sum_{i=1}^A \frac{1}{2} \left[a_0 + a_1 \tau_i^3 \left(1 + \delta a_1(p) - \frac{2g_{\pi p m} F_\pi p^2}{2m g_A (p^2 + m_\pi^2)} + \delta a_1^P(p) \right) \right] \\ &\quad \times \left[\sqrt{L+1} M_{L, L+1}(\mathbf{p}\mathbf{r}_i) + \sqrt{L} M_{L, L-1}(\mathbf{p}\mathbf{r}_i) \right], \end{aligned} \quad (22)$$

$$\begin{aligned} \mathcal{T}_L^{\text{el}5}(p) &= \frac{i}{\sqrt{2L+1}} \\ &\quad \times \sum_{i=1}^A \frac{1}{2} \left[a_0 + a_1 \tau_i^3 \left(1 - 2\frac{p^2}{\Lambda_A^2} + \delta a_1(p) \right) \right] \\ &\quad \times \left[-\sqrt{L} M_{L, L+1}(\mathbf{p}\mathbf{r}_i) + \sqrt{L+1} M_{L, L-1}(\mathbf{p}\mathbf{r}_i) \right], \end{aligned} \quad (23)$$

$$\begin{aligned} \mathcal{T}_L^{\text{mag}5}(p) &= \sum_{i=1}^A \frac{1}{2} \left[a_0 + a_1 \tau_i^3 \left(1 - 2\frac{p^2}{\Lambda_A^2} + \delta a_1(p) \right) \right] \\ &\quad \times M_{L, L}(\mathbf{p}\mathbf{r}_i). \end{aligned} \quad (24)$$

The matrix elements of the operator $M_{L, L'}(\mathbf{p}\mathbf{r}_i) = j_{L'}(\mathbf{p}\mathbf{r}_i) [Y_{L'}(\hat{\mathbf{r}}_i) \boldsymbol{\sigma}_i]^L$ (with L' and $\boldsymbol{\sigma}$ coupled to L) are given in Appendix C.

B. Parity constraints

The different multipoles in Eqs. (22)–(24) have well-defined parity Π , which can be deduced from the definitions given in Appendix B, Eqs. (B6)–(B8), and the transformations under parity of

$$\Pi(\nabla) = -1, \quad \Pi(Y_{LM}) = (-1)^L, \quad \Pi(\mathbf{Y}_{LL}^M) = (-1)^L,$$

and the parity of axial-vector one-body currents $\Pi(\mathbf{J}^A) = +1$. For elastic scattering, where the initial and final states of the nucleus are identical ($J = J_i = J_f$), only the multipoles with positive parity ($\Pi = +1$) contribute to the structure factor, so that we have

$$\begin{aligned}\Pi(\mathcal{L}_L^5) &= (-1)^{L+1} && \Rightarrow L \text{ odd,} \\ \Pi(\mathcal{T}_L^{\text{el}5}) &= (-1)^{L+1} && \Rightarrow L \text{ odd,} \\ \Pi(\mathcal{T}_L^{\text{mag}5}) &= (-1)^L && \Rightarrow L \text{ even.}\end{aligned}$$

Hence, for elastic scattering only the odd- L multipoles of the longitudinal and transverse electric operators and only the even- L multipoles of the transverse magnetic operator contribute. This is also the case for inelastic scattering between initial and final states of the same parity. For inelastic scattering involving different parity states, the above constraints get reversed.

C. Time-reversal constraints

For elastic scattering, time-reversal invariance also constrains the multipoles that contribute to the structure factor. We can write the reduced matrix elements of the sum over one-body operators $O_L(i)$ as [13]

$$\begin{aligned}\langle J \| \sum_{i=1}^A O_L(i) \| J \rangle &\sim \sum_{j,j'} \Psi_J(j,j') \left(\langle j \| O_L \| j' \rangle \right. \\ &\quad \left. + (-1)^{j-j'} \langle j' \| O_L \| j \rangle \right),\end{aligned}\quad (25)$$

where $\Psi_J(j,j')$ denotes the one-body density matrix, and the sum is over single-particle total angular momenta j, j' (for simplicity, we have suppressed the sums over radial quantum numbers n, n' and orbital angular momenta l, l'). Therefore, the symmetry properties of the matrix elements under exchange of initial and final states determine the allowed L contributions to elastic scattering. The relevant operator for SD WIMP-nucleus scattering is $M_{L,L'}$, whose matrix elements are given in Appendix C. They transform as

$$\begin{aligned}\langle n'l' \frac{1}{2} j' \| M_{L,L}(\mathbf{p}\mathbf{r}_i) \| nl \frac{1}{2} j \rangle \\ = (-1)^{j+j'} \langle nl \frac{1}{2} j \| M_{L,L}(\mathbf{p}\mathbf{r}_i) \| n'l' \frac{1}{2} j' \rangle,\end{aligned}\quad (26)$$

$$\begin{aligned}\langle n'l' \frac{1}{2} j' \| M_{L,L\pm 1}(\mathbf{p}\mathbf{r}_i) \| nl \frac{1}{2} j \rangle \\ = (-1)^{j-j'} \langle nl \frac{1}{2} j \| M_{L,L\pm 1}(\mathbf{p}\mathbf{r}_i) \| n'l' \frac{1}{2} j' \rangle.\end{aligned}\quad (27)$$

Therefore, from Eq. (25) it follows that only the multipoles with $M_{L,L\pm 1}$ contribute to elastic scattering. Considering the different multipoles in Eqs. (22)–(24), we thus have

$$\langle J \| \mathcal{T}_L^{\text{mag}5} \| J \rangle = 0, \quad (28)$$

so that the transverse magnetic multipoles do not contribute to elastic scattering.

D. Structure factor for elastic SD scattering

As a result, the structure factor for elastic SD WIMP scattering off nuclei is given by [5]

$$S_A(p) = \sum_{L \text{ odd}} \left(|\langle J \| \mathcal{L}_L^5(p) \| J \rangle|^2 + |\langle J \| \mathcal{T}_L^{\text{el}5}(p) \| J \rangle|^2 \right), \quad (29)$$

and only odd- L longitudinal and electric transverse multipoles contribute.

IV. RESULTS

A. Spectra

The calculation of the structure factors requires a reliable description of the nuclei involved in the scattering process. We perform state-of-the-art large-scale shell-model calculations of the nuclear states using the code ANTOINE [47]. For each nucleus, we solve the many-body problem in an appropriate valence space, which depends on the nuclear mass region. In all calculations, we use nuclear interactions that have been previously employed in nuclear structure and decay studies. To test the quality of the structure calculations, we first compare the theoretical with the experimental spectra for all relevant isotopes.

1. ^{129}Xe , ^{131}Xe , ^{127}I

For the heaviest nuclei for SD WIMP scattering, ^{129}Xe , ^{131}Xe and ^{127}I , the valence space for both protons and neutrons comprises the $0g_{7/2}$, $1d_{5/2}$, $1d_{3/2}$, $2s_{1/2}$, and $0h_{11/2}$ orbitals on top of a ^{100}Sn core. For ^{131}Xe we perform an exact diagonalization in this space. However, in order to make the calculations feasible for ^{129}Xe , the

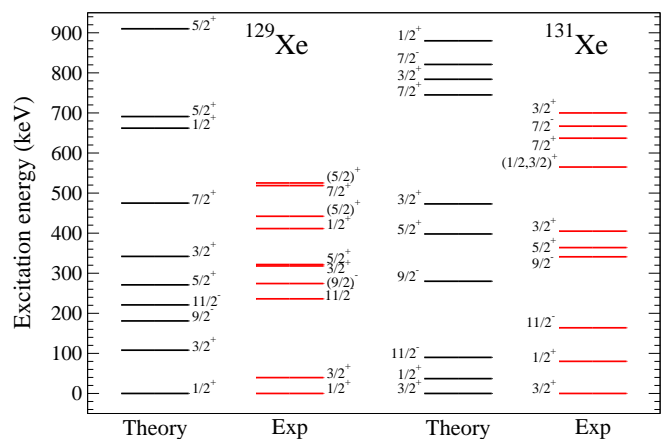


FIG. 1. (Color online) Comparison of calculated spectra of ^{129}Xe and ^{131}Xe with experiment.

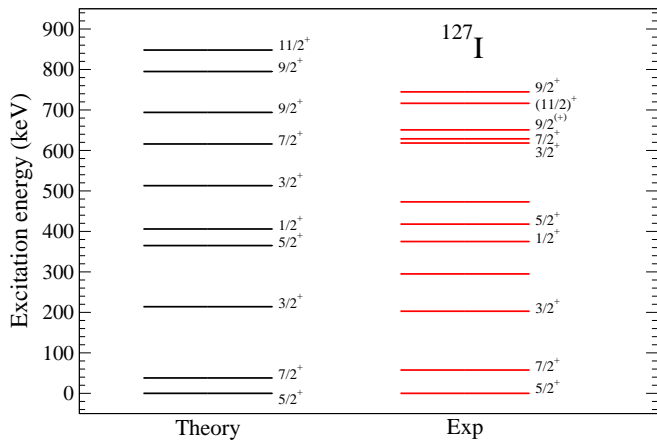


FIG. 2. (Color online) Comparison of the calculated ^{127}I spectrum with experiment.

number of particle excitations from the lower-lying $0g_{7/2}$, $1d_{5/2}$ orbitals into the $1d_{3/2}$, $2s_{1/2}$, and $0h_{11/2}$ orbitals was limited to three. With these restrictions the matrix dimension for this space is 3.5×10^8 . Similarly, for ^{127}I the number of excitations into the $1d_{3/2}$, $2s_{1/2}$, and $0h_{11/2}$ orbitals was limited to four, leading to a matrix dimension of 4.3×10^8 . For this valence space we have used the so-called GCN5082 interaction [48, 49], which is based on a G-matrix with empirical adjustments, mainly in the monopole part, to describe nuclei within this region. The same interaction and valence space have been used to study nuclear structure and double-beta decays in Refs. [48–51].

Figure 1 shows the excitation energies of the lowest-lying states of ^{129}Xe and ^{131}Xe in comparison with experiment (all energies are measured from the ground state). These spectra have been previously presented in Ref. [15]. In Fig. 2, we show the spectrum of ^{127}I . For all three cases, the experimental ground state and the overall ordering of the excited states are very well described. This represents a clear improvement with respect to previous work [23], and validates the interaction and valence space used. Note that for ^{127}I the spin and parity assignment for some experimental states are not known. These states are absent in our calculated spectra, which suggests that they have significant contributions from orbitals lying outside the valence space considered in the present calculations.

2. ^{73}Ge

For ^{73}Ge , the valence space for both protons and neutrons comprises the $1p_{3/2}$, $0f_{5/2}$, $1p_{1/2}$, and $0g_{9/2}$ orbitals on top of a ^{56}Ni core. The calculations are performed in the complete space. We compare results for two different interactions, the so-called GCN2850 interaction [48, 49] (Int. 1 in the following) and the RG inter-

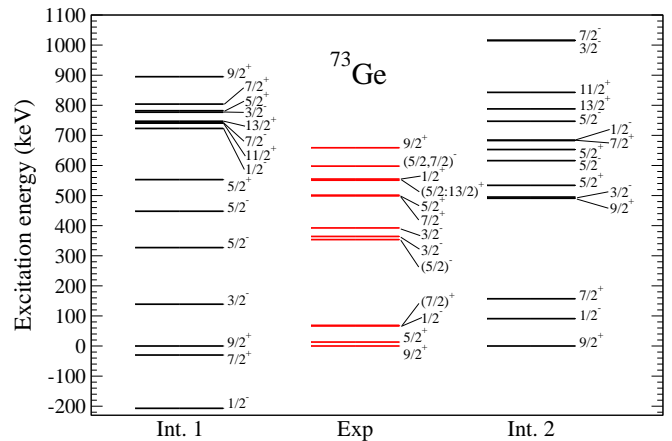


FIG. 3. (Color online) Comparison of calculated ^{73}Ge spectra, using Int. 1 and Int. 2 interactions (for details see text), with experiment.

action [52] (Int. 2). Both are also based on a G-matrix, with mainly monopole empirical adjustments for this region. They have been employed in beta and double-beta decay studies, Refs. [48, 49] for Int. 1 and Refs. [52, 53] for Int. 2. The former was also used in a smaller valence space for the description of ^{73}Ge in Ref. [13].

In Fig. 3 we compare the resulting spectra with experiment. We find that the ground state and the overall ordering of states is much better reproduced by the Int. 2 interaction. In particular, the structure of three of the lowest-lying states and the gap between them and the higher-lying states are well described. In contrast, the Int. 1 interaction predicts a $1/2^-$ ground state, in disagreement with experiment, and the general spacing of the spectrum is not well described. Consequently, the Int. 2 interaction will be the preferred one in this work. Nevertheless, we will also keep the Int. 1 case, in order to study the sensitivity of the structure factor to the different nuclear interactions. It is important to note that the first excited state, which is a $5/2^+$ state, is at too high excitation energy in both calculations. This suggests that an extended valence space, probably including the higher-lying $1d_{5/2}$ orbital, is needed to account for this state. This was also observed in Ref. [17]. A reliable description of the $5/2^+$ state will be crucial for the study of inelastic scattering off ^{73}Ge .

3. ^{19}F , ^{23}Na , ^{27}Al , ^{29}Si

The valence space of the four lighter nuclei ^{19}F , ^{23}Na , ^{27}Al , and ^{29}Si is the sd shell, which comprises the $0d_{5/2}$, $1s_{1/2}$, and $0d_{3/2}$ orbitals, with a ^{16}O core. Full calculations in this valence space are easily performed. In previous works [13, 17, 18, 20, 21], the USD interaction [54] was employed. This interaction consists of a best fit to selected nuclei in this mass region. Here, we use the more

TABLE III. Calculated spin expectation values for protons $\langle \mathbf{S}_p \rangle$ and neutrons $\langle \mathbf{S}_n \rangle$ of $^{129,131}\text{Xe}$, ^{127}I , ^{73}Ge , ^{29}Si , ^{27}Al , ^{23}Na , and ^{19}F , compared to the previous calculations of Refs. [13, 17–23].

	^{129}Xe		^{131}Xe		^{127}I		^{73}Ge		^{29}Si		^{27}Al		^{23}Na		^{19}F	
	$\langle \mathbf{S}_n \rangle$	$\langle \mathbf{S}_p \rangle$	$\langle \mathbf{S}_n \rangle$	$\langle \mathbf{S}_p \rangle$	$\langle \mathbf{S}_n \rangle$	$\langle \mathbf{S}_p \rangle$	$\langle \mathbf{S}_n \rangle$	$\langle \mathbf{S}_p \rangle$	$\langle \mathbf{S}_n \rangle$	$\langle \mathbf{S}_p \rangle$	$\langle \mathbf{S}_n \rangle$	$\langle \mathbf{S}_p \rangle$	$\langle \mathbf{S}_n \rangle$	$\langle \mathbf{S}_p \rangle$	$\langle \mathbf{S}_n \rangle$	$\langle \mathbf{S}_p \rangle$
This work	0.329	0.010	-0.272	-0.009	0.031	0.342	0.439	0.031	0.156	0.016	0.038	0.326	0.024	0.224	-0.002	0.478
(Int. 1)							0.450	0.006								
[20] (Bonn A)	0.359	0.028	-0.227	-0.009	0.075	0.309							0.020	0.248		
[20] (Nijm. II)	0.300	0.013	-0.217	-0.012	0.064	0.354										
[18]											0.030	0.343				
[17]							0.468	0.011	0.13	-0.002						
[19]							0.378	0.030								
[23]	0.273	-0.002	-0.125	$-7 \cdot 10^{-4}$	0.030	0.418										
[22]					0.038	0.330	0.407	0.005					0.020	0.248		
[21]									0.133	-0.002			0.020	0.248	-0.009	0.475
[13]	0.248	0.007	-0.199	-0.005	0.066	0.264	0.475	0.008					0.020	0.248	-0.009	0.475

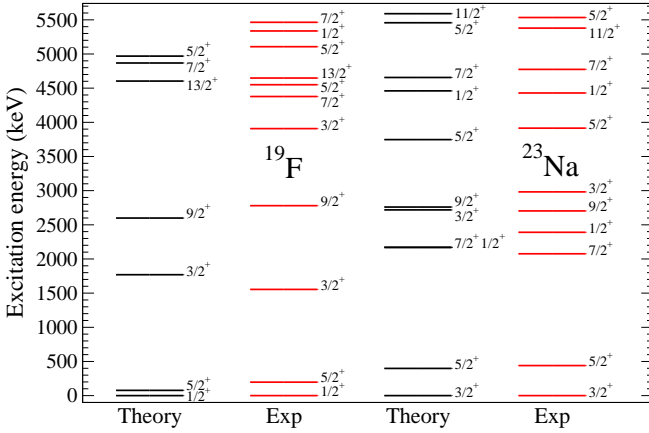


FIG. 4. (Color online) Comparison of calculated spectra of ^{19}F and ^{23}Na with experiment.

recent USDB interaction [55], which is an improved version of USD. The difference between the two interactions is small, see Sec. IV B. In Figs. 4 and 5 the positive-parity excited states of all four nuclei are shown compared to experiment (in the sd shell only positive-parity states can be obtained). The agreement with experiment is very good in all cases, both for the ordering and the quantitative reproduction of the excitation energies.

B. Spin expectation values

In the limit of low momentum transfer, $p = 0$, the structure factor for elastic SD WIMP scattering is given by the proton and neutron spins $\mathbf{S}_p = \sum_{i=1}^Z \boldsymbol{\sigma}_i/2$ and

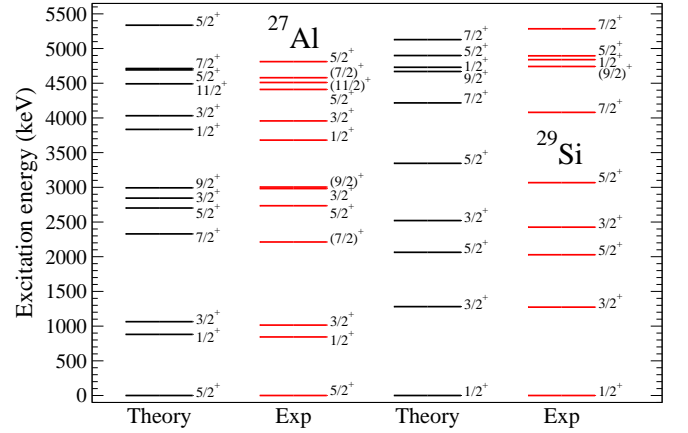


FIG. 5. (Color online) Comparison of calculated spectra of ^{27}Al and ^{29}Si with experiment.

$\mathbf{S}_n = \sum_{i=1}^N \boldsymbol{\sigma}_i/2$ in the nucleus [5]:

$$\begin{aligned}
 S_A(0) &= \frac{1}{4\pi} |(a_0 + a'_1) \langle J \| \mathbf{S}_p \| J \rangle + (a_0 - a'_1) \langle J \| \mathbf{S}_n \| J \rangle|^2 \\
 &= \frac{(2J+1)(J+1)}{4\pi J} |(a_0 + a'_1) \langle \mathbf{S}_p \rangle + (a_0 - a'_1) \langle \mathbf{S}_n \rangle|^2,
 \end{aligned}
 \tag{30}$$

where $a'_1 = a_1(1 + \delta a_1(0))$ includes the effects from chiral 2b currents. The spin expectation values are defined as $\langle \mathbf{S}_{n,p} \rangle = \langle JM = J | \mathbf{S}_{n,p}^3 | JM = J \rangle$.

We list our calculated spin expectation values $\langle \mathbf{S}_{n,p} \rangle$ in Table III in comparison to previous calculations. As expected for odd-mass nuclei with even number of protons ($^{129,131}\text{Xe}$, ^{73}Ge , and ^{29}Si) $|\langle \mathbf{S}_n \rangle| \gg |\langle \mathbf{S}_p \rangle|$, while for odd-mass nuclei with an even number of neutrons (^{19}F , ^{23}Na , ^{27}Al , and ^{127}I) $|\langle \mathbf{S}_n \rangle| \ll |\langle \mathbf{S}_p \rangle|$. As a result, the WIMP coupling to the even species will be suppressed.

Moreover, the sensitivity to the precise value of the even neutrons spin is very weak when chiral 2b currents are included. This is shown in Sec. IV C. Chiral 2b currents lead to an interaction of neutrons and protons that overwhelms the direct WIMP coupling to the suppressed spin expectation value, so that the structure factors are almost entirely determined by the dominant $\langle \mathbf{S}_{n/p} \rangle$ (for odd neutron/proton isotopes).

The spin expectation values of the lighter nuclei, ^{19}F , ^{23}Na , ^{27}Al , and ^{29}Si in Table III are very close to those of Refs. [13, 17, 18, 20, 21] due to the similarity of the USD and USDB interactions. This indicates that the structure for these nuclei is under good control. For ^{73}Ge we find a weak sensitivity of the dominant $\langle \mathbf{S}_n \rangle$ value comparing the preferred Int. 2 interaction (“This work”) to the Int. 1 interaction. This range is smaller than the one in previous calculations of Refs. [13, 17, 19, 22], suggesting that the latter may have an even larger variation in the spectra due to truncations or deficiencies in the interactions used. Also for the heavier nuclei, $^{129,131}\text{Xe}$, and ^{127}I , we have performed calculations in the largest spaces to date and with tested interactions. For $^{129,131}\text{Xe}$, the comparison to previous results is discussed in detail in Ref. [15]. For the dominant $\langle \mathbf{S}_n \rangle$ values for $^{129,131}\text{Xe}$, and the dominant $\langle \mathbf{S}_p \rangle$ value for ^{127}I , the difference to previous calculations of Refs. [13, 20, 22, 23] is about 25% (and 55% for ^{131}Xe). We attribute these differences to the sizable truncations of the valence spaces in those calculations and because the interactions used have not been as well tested.

C. Structure factors

1. Isoscalar/isovector versus proton/neutron

The structure factor $S_A(p)$ can be decomposed in terms of its isoscalar and isovector parts $S_{ij}(p)$, characterized by the isoscalar and isovector couplings a_0 and a_1 :

$$S_A(p) = a_0^2 S_{00}(p) + a_0 a_1 S_{01}(p) + a_1^2 S_{11}(p). \quad (32)$$

However, it is common in the literature to use the structure factors $S_p(p)$ and $S_n(p)$, which are referred to as “proton-only” and “neutron-only”, respectively. They are defined by the couplings $a_0 = a_1 = 1$ (“proton-only”) and $a_0 = -a_1 = 1$ (“neutron-only”) and are thus related to the isoscalar and isovector structure factors by

$$S_p(p) = S_{00}(p) + S_{01}(p) + S_{11}(p), \quad (33)$$

$$S_n(p) = S_{00}(p) - S_{01}(p) + S_{11}(p). \quad (34)$$

The origin of the “proton/neutron-only” structure factors can be understood from Eq. (31). When 2b currents are neglected, at $p = 0$ the “proton/neutron-only” structure factors are determined entirely by the proton/neutron spin expectation values. Moreover, when the higher-order isovector parts in 1b currents are neglected, this separation also holds for $p > 0$. Because

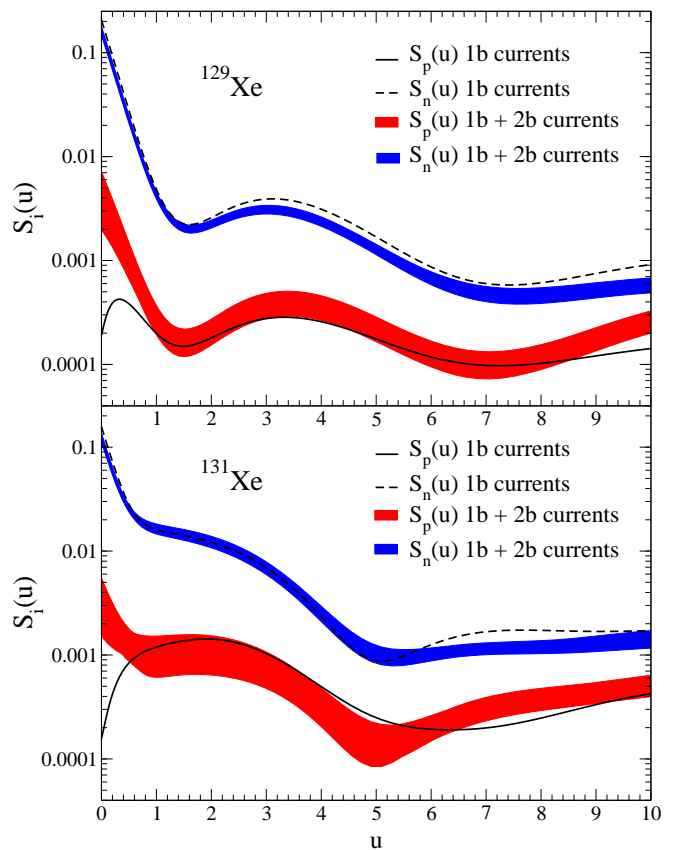


FIG. 6. (Color online) Structure factors $S_p(u)$ (solid lines) and $S_n(u)$ (dashed) for ^{129}Xe (top panel) and ^{131}Xe (bottom panel) as a function of $u = p^2 b^2 / 2$. The harmonic-oscillator lengths are $b = 2.2853$ fm and $b = 2.2905$ fm for ^{129}Xe and ^{131}Xe , respectively. Results are shown at the 1b current level, and also including 2b currents. The estimated theoretical uncertainty is given by the red ($S_p(u)$) and blue ($S_n(u)$) bands.

for odd-mass nuclei there is a clear hierarchy of the spin expectation values (with either $|\langle \mathbf{S}_n \rangle| \gg |\langle \mathbf{S}_p \rangle|$ or $|\langle \mathbf{S}_p \rangle| \gg |\langle \mathbf{S}_n \rangle|$), the proton/neutron decomposition is useful to capture the dominant parts of $S_A(p)$. For this reason, and because it is common experimentally, we will also largely consider the proton/neutron decomposition here. This is merely a convenient choice of a_0, a_1 couplings, but the notation “proton/neutron-only” is misleading, because it does not imply that the coupling is to protons/neutrons only. Strong interactions between nucleons in 2b currents, as well as the isovector nature of pseudo-scalar and other Q^2 1b currents, mean that WIMPs effectively couple to protons and neutrons in nuclei. In fact, with 2b currents, both $S_p(p)$ and $S_n(p)$ are determined by the spin distribution of the odd species.

In the following, we present structure factors as a function of $u = p^2 b^2 / 2$ with harmonic-oscillator length $b = (\hbar/m\omega)^{1/2}$ and $\hbar\omega = (45A^{-1/3} - 25A^{-2/3})$ MeV. When 2b currents are included, we provide theoretical error bands due to the uncertainties in WIMP currents

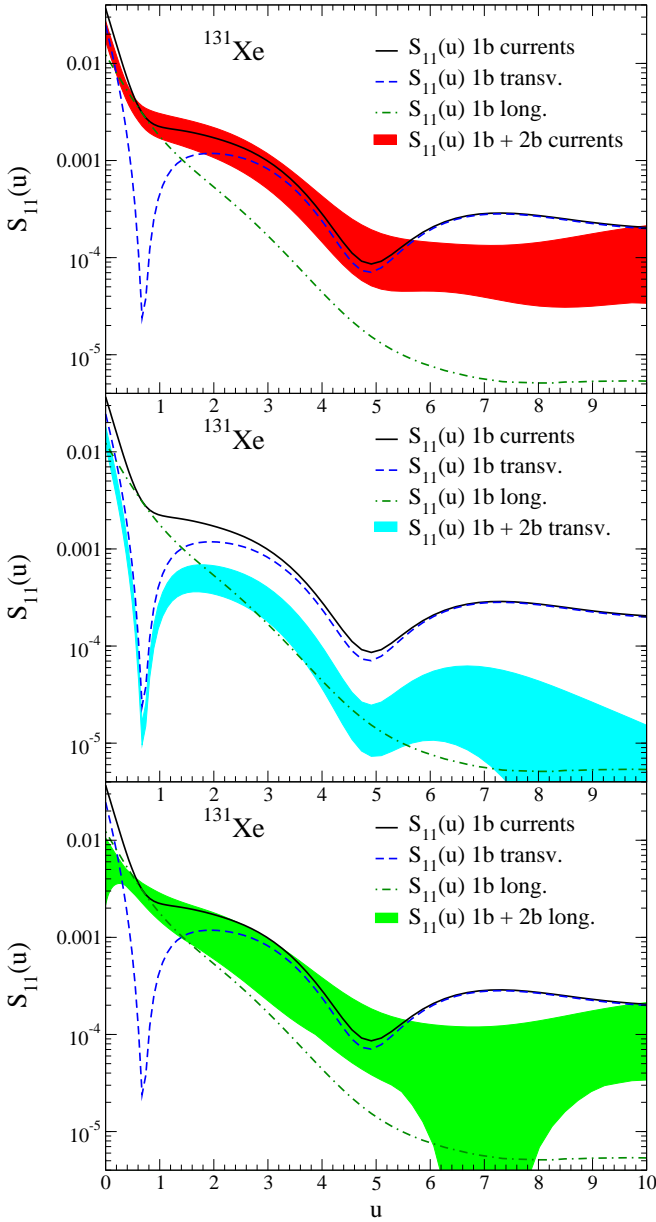


FIG. 7. (Color online) Decomposition of the isovector structure factor $S_{11}(u)$ for ^{131}Xe . At the 1b current level, the full result (solid, black lines) and the contributions from transverse electric (dashed, blue) and from longitudinal (dot-dashed, green) multipoles are shown. The top panel gives also the full 1b plus 2b current result (red band), while the middle/bottom panels show the 1b plus 2b results when only transverse/longitudinal multipoles are included (blue/green band). The bands give the estimated 2b-current uncertainty.

in nuclei, see Table II. This takes into account the uncertainties in the low-energy couplings c_3, c_4 and in the density range $\rho = 0.10 \dots 0.12 \text{ fm}^{-3}$.

For ^{129}Xe and ^{131}Xe the predicted isoscalar/isovector structure factors $S_{00}(u), S_{01}(u)$, and $S_{11}(u)$ were discussed in detail in Ref. [15], and they were compared

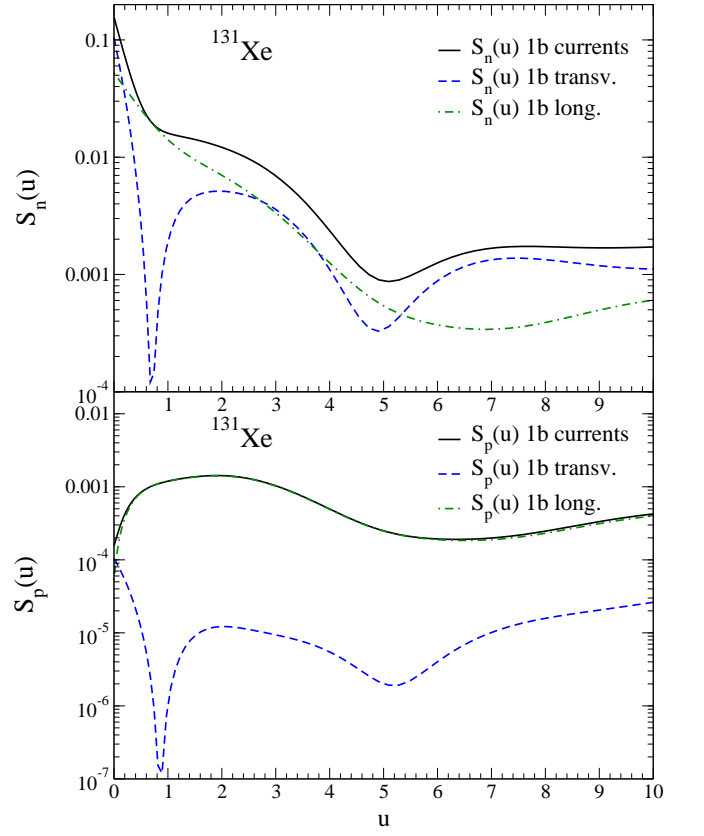


FIG. 8. (Color online) Structure factors $S_n(u)$ (top panel) and $S_p(u)$ (bottom panel) for ^{131}Xe . At the 1b current level, the full results (solid, black lines) are compared with the contributions from transverse electric (dashed, blue) and from longitudinal (dot-dashed, green) multipoles.

to the previous calculations of Refs. [20, 23] (see also Sec. IV B). Here, we present in Fig. 6 the proton/neutron structure factors $S_p(u)$. At the 1b current level, the results at $p = 0$ are determined by the spin expectation values. Chiral 2b currents provide important contributions to the structure factors, especially for $p \lesssim 100 \text{ MeV}$, where we find in Fig. 6 a significant increase of $S_p(u)$. This is because with 2b currents, neutrons can contribute to the “proton-only” ($a_0 = a_1 = 1$) coupling due to the axial $\delta a_1(p)$ contribution in Eq. (31). For $S_n(u)$, 2b currents lead to a small reduction in the structure factor, depending on the momentum transfer. This is caused by the combined effect of the axial $\delta a_1(p)$ and the pseudoscalar $\delta a_1^P(p)$ contributions. To better understand how these different contributions enter, we study a multipole decomposition of the structure factors.

2. Multipole decomposition

In Fig. 7 we show the transverse/longitudinal decomposition of the results with 1b as well as 1b plus 2b currents for the isovector structure factor $S_{11}(u)$ of ^{131}Xe

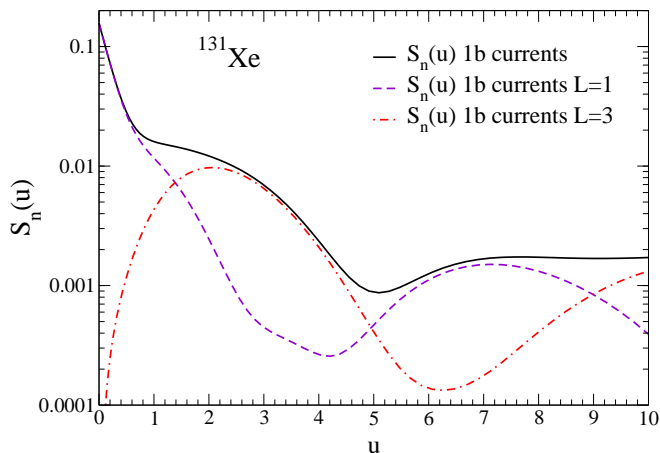


FIG. 9. (Color online) Decomposition at the 1b current level of the ^{131}Xe structure factor $S_n(u)$ (solid, black line) in $L = 1$ (dashed, violet) and $L = 3$ (dot-dashed, orange) multipoles.

(the long-range 2b currents are isovector). The different 2b current contributions can be clearly seen in Fig. 7. In the middle panel, where only the transverse electric multipoles are taken into account, 2b currents reduce the 1b result due to the negative axial $\delta a_1(p)$ values in Table II. We observe that the relative reduction depends on u and becomes more important at higher momentum transfer. The bottom panel shows the longitudinal multipoles, where both axial $\delta a_1(p)$ and pseudo-scalar $\delta a_1^P(p)$ 2b current contributions enter. At zero momentum transfer we find a reduction of the structure factor, driven by $\delta a_1(p)$, but at $u \sim 0.7$, $p \sim 100$ MeV, this turns into an enhancement due to $\delta a_1^P(p)$. In the upper panel, the full 1b plus 2b band is given, where the final reduction or enhancement over the 1b result, for a given u value, depends on the relative impact of the transverse electric and longitudinal multipoles.

It is interesting to study the transverse/longitudinal decomposition at the 1b level, as shown in Fig. 8 for $S_n(u)$ and $S_p(u)$ of ^{131}Xe . While both multipoles contribute to $S_n(u)$ (their relative importance depends on u), $S_p(u)$ is completely dominated by the longitudinal multipoles except at $p = 0$. In ^{131}Xe almost all of the spin is carried by neutrons, so $S_p(0)$ is very small at the 1b level. However, for $p > 0$ the (isovector) pseudo-scalar currents allow neutrons to contribute to $S_p(u)$, leading to a steep increase in the longitudinal contribution to $S_p(u)$. Because pseudo-scalar currents only contribute to the longitudinal multipoles, the transverse part from the protons also remains very small for $p > 0$.

Another way to decompose the structure factors is in terms of the different L values of the multipoles. Because the ground state of ^{129}Xe is $1/2^+$, only $L = 1$ contributes. For ^{131}Xe , with a $3/2^+$ ground state, $L = 1$ and $L = 3$ multipoles enter (even- L multipoles are forbidden due to parity, see Sec. III B). The L decomposition of the ^{131}Xe structure factor $S_n(u)$ is shown in Fig. 9, for simplicity

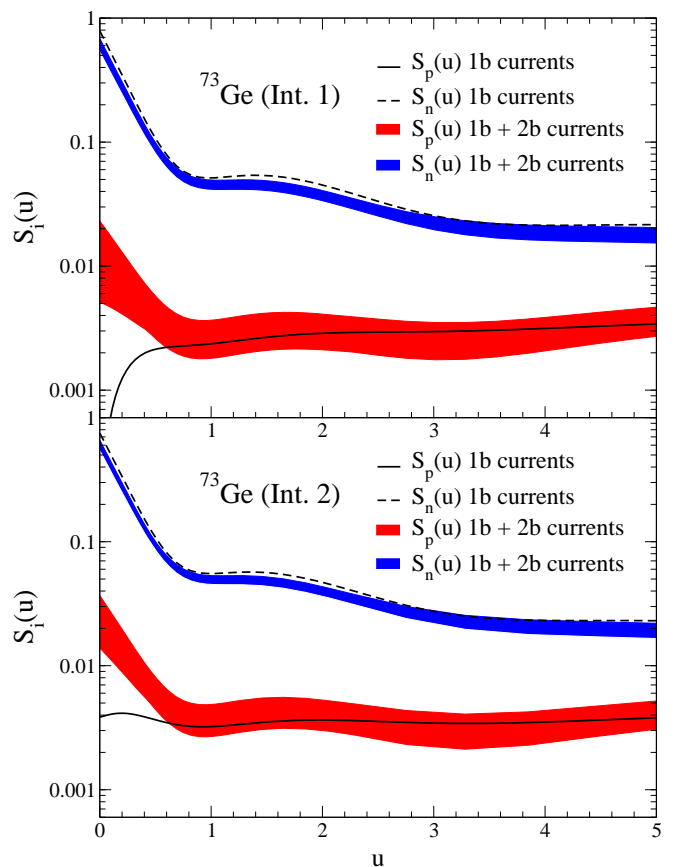


FIG. 10. (Color online) Structure factors $S_p(u)$ (solid lines) and $S_n(u)$ (dashed) for ^{73}Ge calculated using the Int. 1 (GCN5028, top panel) and the Int. 2 interaction (RG, bottom panel) as a function of $u = p^2 b^2 / 2$ with $b = 2.1058$ fm. Results are shown at the 1b current level, and also including 2b currents. The estimated theoretical uncertainty is given by the red ($S_p(u)$) and blue ($S_n(u)$) bands.

at the 1b current level. We observe that the $L = 3$ multipoles dominate for $1.5 \lesssim u \lesssim 5$. As a result, the structure factors fall off considerably more slowly for ^{131}Xe compared to ^{129}Xe , where only $L = 1$ contributes.

3. ^{73}Ge

Figure 10 shows the structure factors for ^{73}Ge for the different Int. 1 and Int. 2 interactions (the latter is preferred based on the spectra, see Fig. 3). The structure factor $S_n(u)$ differs by less than 10% between the two interactions. At the 1b current level, $S_p(u)$ for low momentum transfers is substantially smaller for Int. 1, due to the very small $\langle \mathbf{S}_p \rangle$ value. However, when 2b currents are included, also for $S_p(u)$ the contributions from neutrons are dominant, which translates to similar structure factors for the two interactions. This is because of the similar $\langle \mathbf{S}_n \rangle$ values (see Table III) combined with the neutron-proton coupling through 2b currents.

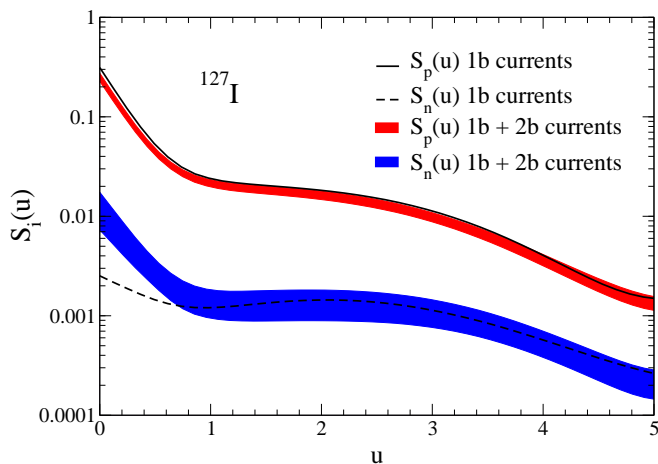


FIG. 11. (Color online) Structure factors $S_p(u)$ (solid lines) and $S_n(u)$ (dashed) for ^{127}I as a function of $u = p^2 b^2/2$ with $b = 2.2801$ fm. Results are shown at the 1b current level, and also including 2b currents. The estimated theoretical uncertainty is given by the red ($S_p(u)$) and blue ($S_n(u)$) bands.

4. ^{127}I , ^{19}F , ^{23}Na , ^{27}Al , ^{29}Si

In Figs. 11, 12, and 13, we show the structure factors $S_n(u)$ and $S_p(u)$ for ^{127}I , ^{19}F , ^{23}Na , ^{27}Al , and ^{29}Si at the 1b current level and including 2b currents. The dominant structure factor is the one for the odd species. Therefore, for ^{29}Si $S_n(u)$ dominates, while for the other isotopes $S_p(u)$ is the main component. All the features discussed for ^{131}Xe in Sec. IV C 2 translate to these isotopes as well: The structure factors for the nondominant “proton/neutron-only” couplings are strongly increased when 2b currents are included. For the dominant structure factor, 2b currents produce a reduction, by about 10% – 30% at low momentum transfers, which at large u can turn into a weak enhancement due to the 2b current contribution to the pseudo-scalar currents. This is most clearly seen for ^{19}F in the top panel of Fig. 12, where we also show the isoscalar/isovector structure factors $S_{00}(u)$, $S_{01}(u)$, and $S_{11}(u)$. Note that the structure factor $S_{01}(u)$ vanishes at the point where $S_p(u)$ and $S_n(u)$ cross.

V. CONCLUSIONS AND OUTLOOK

This work presents a comprehensive derivation of SD WIMP scattering off nuclei based on chiral EFT, including one-body currents to order Q^2 and the long-range Q^3 two-body currents due to pion exchange, which are predicted in chiral EFT. Two-body currents are the leading corrections to the couplings of WIMPs to single nucleons, assumed in all previous studies. Combined with detailed Appendixes, we have presented the general formalism necessary to describe both elastic and inelastic WIMP-nucleus scattering.

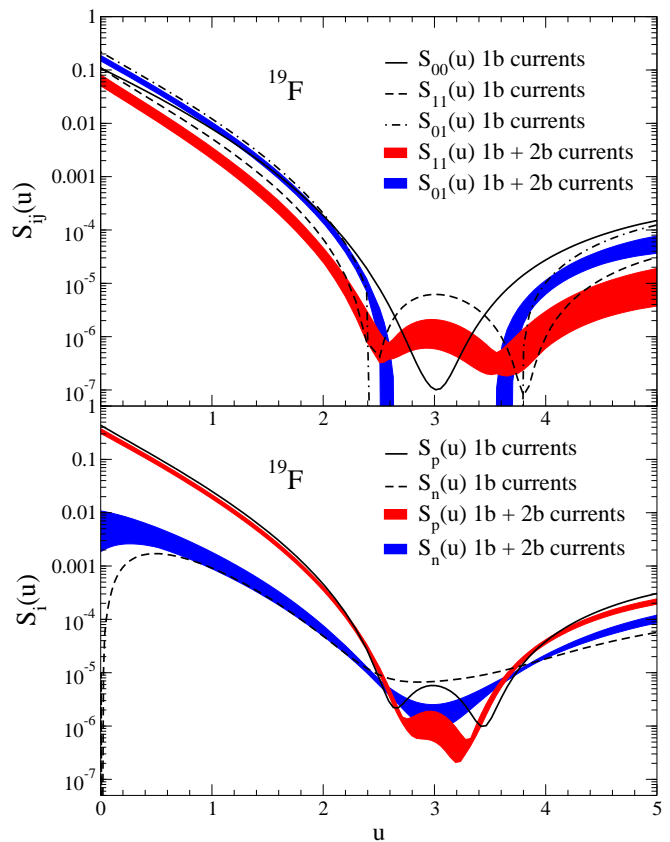


FIG. 12. (Color online) Structure factors for ^{19}F as a function of $u = p^2 b^2/2$ with $b = 1.7608$ fm. Top panel: Isoscalar/isovector $S_{00}(u)$ (solid line), $S_{01}(u)$ (dashed), and $S_{11}(u)$ (dot-dashed) decomposition. Bottom panel: Proton/neutron $S_p(u)$ (solid line) and $S_n(u)$ (dashed) decomposition. In both panels results are shown at the 1b current level, and also including 2b currents. The estimated theoretical uncertainty is given by the red ($S_{11}(u)$, $S_p(u)$) and blue ($S_{01}(u)$, $S_n(u)$) bands.

We have performed state-of-the-art large-scale shell-model calculations for all nonzero-spin nuclei relevant to direct dark matter detection, using the largest valence spaces accessible with nuclear interactions that have been tested in nuclear structure and decay studies. The comparison of theoretical and experimental spectra demonstrate a good description of these isotopes. We have calculated the structure factors for elastic SD WIMP scattering for all cases using chiral EFT currents, including theoretical error bands due to the nuclear uncertainties of WIMP currents in nuclei. Fits for the structure factors are given in Appendix D.

We have studied in detail the role of two-body currents, the contributions of different multipole operators, and the issue of proton/neutron versus isoscalar/isovector decompositions of the structure factors. The long-range two-body currents reduce the isovector parts of the structure factor at low momentum transfer, while they can lead to a weak enhancement at higher momentum trans-

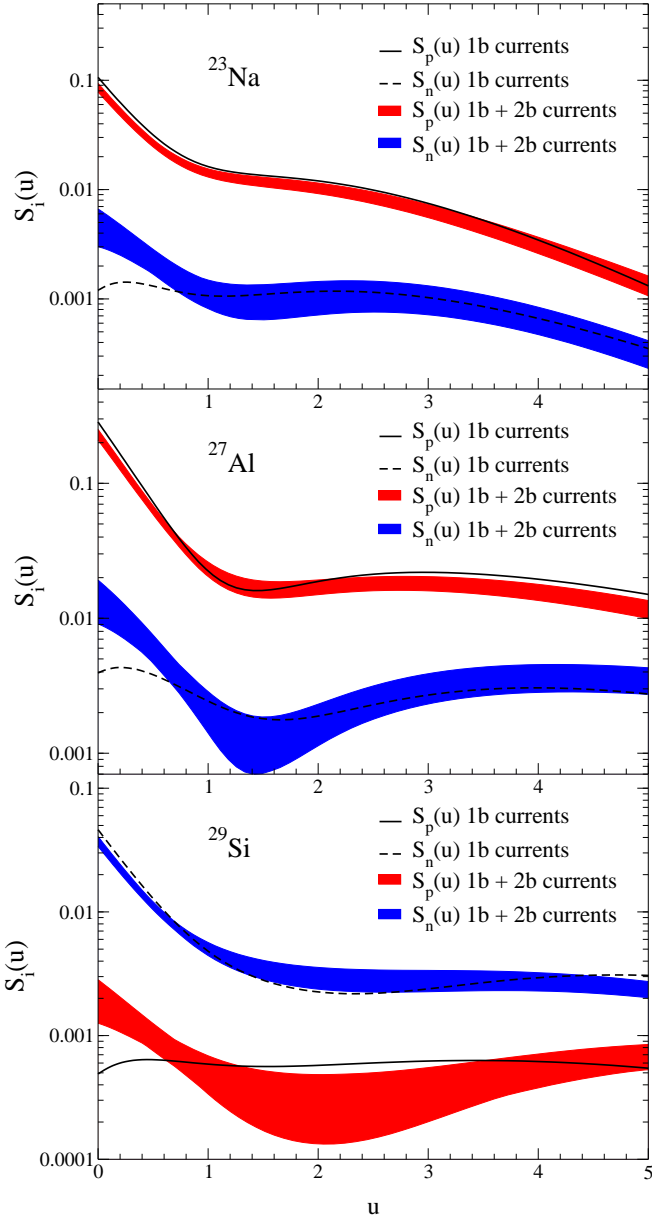


FIG. 13. (Color online) Structure factors $S_p(u)$ (solid lines) and $S_n(u)$ (dashed) for ^{23}Na (top panel), ^{27}Al (middle panel), and ^{29}Si (bottom panel) as a function of $u = p^2 b^2 / 2$, with harmonic-oscillator lengths $b = 1.8032$ fm (^{23}Na), $b = 1.8405$ fm (^{27}Al), and $b = 1.8575$ fm (^{29}Si). Results are shown at the 1b current level, and also including 2b currents. The estimated theoretical uncertainty is given by the red ($S_p(u)$) and blue ($S_n(u)$) bands.

fers. Moreover, we have shown that for odd-neutron (odd-proton) nuclei, two-body currents lead to a significant increase of the “proton-only” (“neutron-only”) structure factors, because of strong interactions between nucleons through two-body currents that allow the odd species carrying most of the spin to contribute. This implies that WIMPs effectively couple to protons and neu-

trons in nuclei, so that the notation “proton/neutron-only” is misleading. In fact, with 2b currents, both “proton/neutron-only” structure factors are determined by the spin distribution of the odd species.

Future improvements of the nuclear physics of dark matter detection includes developing shell-model interactions based on chiral EFT, where the present frontier are semi-magic nuclei up to the calcium region [56–61], *ab-initio* benchmarks for the lightest isotope ^{19}F , and expanding the valences spaces (especially for germanium). In addition, a full treatment of the one- and two-body currents would require to renormalize them to the valence space of the many-body calculation, which can lead to additional contributions to the currents. This and going beyond the normal-ordering approximation will be pursued in future work. Moreover, we plan to investigate other responses [13] based on the same large-scale nuclear-structure calculations presented here.

ACKNOWLEDGEMENTS

We thank L. Baudis, J. Engel, W. C. Haxton, R. F. Lang, T. Marrodan, and T. S. Park for helpful discussions. This work was supported by ARCHES, by the DFG through Grant No. SFB 634, and by the Helmholtz Alliance Program of the Helmholtz Association, contract HA216/EMMI “Extremes of Density and Temperature: Cosmic Matter in the Laboratory”.

Appendix A: Calculation of the effective one-body current $\mathbf{J}_{i,2b}^{\text{eff}}$

We calculate the normal-ordered 1b part of 2b currents by summing the second nucleon over occupied states of a spin and isospin symmetric reference state or core, which we take as a Fermi gas:

$$\mathbf{J}_{i,2b}^{\text{eff}} = \sum_j (1 - P_{ij}) \mathbf{J}_{ij}^3, \quad (\text{A1})$$

where the sum is over occupied states, \mathbf{J}_{ij}^3 is the 2b current defined in Eq. (8), and P_{ij} is the exchange operator. In this approximation, the momenta \mathbf{k}_1 and \mathbf{k}_2 in the direct (d) and exchange (ex) contributions are given by

$$\mathbf{k}_i^{\text{d}} = \mathbf{p}'_i - \mathbf{p}_i = -\mathbf{p}, \quad (\text{A2})$$

$$\mathbf{k}_i^{\text{ex}} = P_{ij}^k \mathbf{k}_i^{\text{d}} = \mathbf{p}_j - \frac{\mathbf{P} + \mathbf{p}}{2}, \quad (\text{A3})$$

$$\mathbf{k}_j^{\text{d}} = \mathbf{p}'_j - \mathbf{p}_j = 0, \quad (\text{A4})$$

$$\mathbf{k}_j^{\text{ex}} = P_{ij}^k \mathbf{k}_j^{\text{d}} = -\mathbf{p}_j + \frac{\mathbf{P} - \mathbf{p}}{2}, \quad (\text{A5})$$

where we have used that the initial and final momenta of the nucleon in the occupied state are identical, $\mathbf{p}_j = \mathbf{p}'_j$.

The nonvanishing contributions to $\mathbf{J}_{i,2b}^{\text{eff}}$ can be grouped into five terms, arising from Eq. (8): the di-

rect (d) and exchange (ex) terms of the c_3 term, as well as from the exchange c_4 , p_1 , and \hat{c}_6 terms. They read

$$\mathbf{J}_{i,2b}^{\text{eff,d}}(c_3 \text{ term}) = -\frac{g_A}{F_\pi^2} \frac{\tau_i^3}{2} \frac{8}{(2\pi)^3} \int_0^{k_F} \frac{c_3}{m_\pi^2 + \mathbf{p}^2} (\mathbf{p} \cdot \boldsymbol{\sigma}_i) \mathbf{p} d^3 \mathbf{p}_j = -\frac{g_A \rho}{F_\pi^2} \frac{\tau_i^3}{2} 2c_3 \frac{(\mathbf{p} \cdot \boldsymbol{\sigma}_i) \mathbf{p}}{m_\pi^2 + \mathbf{p}^2}, \quad (\text{A6})$$

$$\begin{aligned} \mathbf{J}_{i,2b}^{\text{eff,ex}}(c_3 \text{ term}) &= -\frac{g_A}{F_\pi^2} \frac{\tau_i^3}{2} \frac{4}{(2\pi)^3} \frac{1}{2} \left[\int_0^{k_F} \frac{c_3}{m_\pi^2 + (\mathbf{k}_i^{\text{ex}})^2} (\mathbf{k}_i^{\text{ex}} \cdot \boldsymbol{\sigma}_i) \mathbf{k}_i^{\text{ex}} d^3 \mathbf{p}_j + \int_0^{k_F} \frac{c_3}{m_\pi^2 + (\mathbf{k}_j^{\text{ex}})^2} (\mathbf{k}_j^{\text{ex}} \cdot \boldsymbol{\sigma}_i) \mathbf{k}_j^{\text{ex}} d^3 \mathbf{p}_j \right] \\ &= -\frac{g_A \rho}{F_\pi^2} \frac{\tau_i^3}{2} \frac{1}{6} c_3 \left[I_1^\sigma(\rho, |\mathbf{P} - \mathbf{p}|) \boldsymbol{\sigma}_i + I^P(\rho, |\mathbf{P} - \mathbf{p}|) ((\widehat{\mathbf{P} - \mathbf{p}}) \cdot \boldsymbol{\sigma}_i) (\widehat{\mathbf{P} - \mathbf{p}}) + I_1^\sigma(\rho, |\mathbf{P} + \mathbf{p}|) \boldsymbol{\sigma}_i \right. \\ &\quad \left. + I^P(\rho, |\mathbf{P} + \mathbf{p}|) ((\widehat{\mathbf{P} + \mathbf{p}}) \cdot \boldsymbol{\sigma}_i) (\widehat{\mathbf{P} + \mathbf{p}}) \right], \quad (\text{A7}) \end{aligned}$$

$$\begin{aligned} \mathbf{J}_{i,2b}^{\text{eff,ex}}(c_4 \text{ term}) &= \frac{g_A}{F_\pi^2} \frac{\tau_i^3}{2} \left(c_4 + \frac{1}{4m} \right) \frac{4}{(2\pi)^3} \frac{1}{2} \left[\int_0^{k_F} \frac{1}{m_\pi^2 + (\mathbf{k}_i^{\text{ex}})^2} \mathbf{k}_i^{\text{ex}} \times (\boldsymbol{\sigma}_i \times \mathbf{k}_i^{\text{ex}}) d^3 \mathbf{p}_j \right. \\ &\quad \left. + \int_0^{k_F} \frac{1}{m_\pi^2 + (\mathbf{k}_j^{\text{ex}})^2} \mathbf{k}_j^{\text{ex}} \times (\boldsymbol{\sigma}_i \times \mathbf{k}_j^{\text{ex}}) d^3 \mathbf{p}_j \right] \\ &= \frac{g_A \rho}{F_\pi^2} \frac{\tau_i^3}{2} \frac{1}{6} \left(c_4 + \frac{1}{4m} \right) \left[\left(3I_2^\sigma(\rho, |\mathbf{P} - \mathbf{p}|) - I_1^\sigma(\rho, |\mathbf{P} - \mathbf{p}|) + 3I_2^\sigma(\rho, |\mathbf{P} + \mathbf{p}|) - I_1^\sigma(\rho, |\mathbf{P} + \mathbf{p}|) \right) \boldsymbol{\sigma}_i \right. \\ &\quad \left. - I^P(\rho, |\mathbf{P} - \mathbf{p}|) ((\widehat{\mathbf{P} - \mathbf{p}}) \cdot \boldsymbol{\sigma}_i) (\widehat{\mathbf{P} - \mathbf{p}}) - I^P(\rho, |\mathbf{P} + \mathbf{p}|) ((\widehat{\mathbf{P} + \mathbf{p}}) \cdot \boldsymbol{\sigma}_i) (\widehat{\mathbf{P} + \mathbf{p}}) \right], \quad (\text{A8}) \end{aligned}$$

$$\begin{aligned} \mathbf{J}_{i,2b}^{\text{eff,ex}}(p_1 \text{ term}) &= \frac{g_A}{mF_\pi^2} \frac{\tau_i^3}{2} \frac{4}{(2\pi)^3} \frac{1}{8} \left[\int_0^{k_F} \frac{(\mathbf{p}_j + \frac{\mathbf{P} - \mathbf{p}}{2}) (\boldsymbol{\sigma}_i \cdot \mathbf{k}_i^{\text{ex}})}{m_\pi^2 + (\mathbf{k}_i^{\text{ex}})^2} d^3 \mathbf{p}_j - \int_0^{k_F} \frac{(\mathbf{p}_j + \frac{\mathbf{P} + \mathbf{p}}{2}) (\boldsymbol{\sigma}_i \cdot \mathbf{k}_j^{\text{ex}})}{m_\pi^2 + (\mathbf{k}_j^{\text{ex}})^2} d^3 \mathbf{p}_j \right] \\ &= \frac{g_A \rho}{mF_\pi^2} \frac{\tau_i^3}{2} \frac{1}{24} \left[I_1^\sigma(\rho, |\mathbf{P} - \mathbf{p}|) \boldsymbol{\sigma}_i + I_1^P(\rho, |\mathbf{P} - \mathbf{p}|) ((\widehat{\mathbf{P} - \mathbf{p}}) \cdot \boldsymbol{\sigma}_i) (\widehat{\mathbf{P} - \mathbf{p}}) \right. \\ &\quad \left. + \frac{|\mathbf{p}|}{|\mathbf{P} - \mathbf{p}|} I_2^\sigma(\rho, |\mathbf{P} - \mathbf{p}|) ((\widehat{\mathbf{P} - \mathbf{p}}) \cdot \boldsymbol{\sigma}_i) (\hat{\mathbf{p}}) - \frac{1}{4} \frac{|\mathbf{P} + \mathbf{p}|}{|\mathbf{P} - \mathbf{p}|} I_4^P(\rho, |\mathbf{P} - \mathbf{p}|) ((\widehat{\mathbf{P} - \mathbf{p}}) \cdot \boldsymbol{\sigma}_i) (\widehat{\mathbf{P} + \mathbf{p}}) \right. \\ &\quad \left. + I_1^\sigma(\rho, |\mathbf{P} + \mathbf{p}|) \boldsymbol{\sigma}_i + I_1^P(\rho, |\mathbf{P} + \mathbf{p}|) ((\widehat{\mathbf{P} + \mathbf{p}}) \cdot \boldsymbol{\sigma}_i) (\widehat{\mathbf{P} + \mathbf{p}}) \right. \\ &\quad \left. - \frac{|\mathbf{p}|}{|\mathbf{P} + \mathbf{p}|} I_2^\sigma(\rho, |\mathbf{P} + \mathbf{p}|) ((\widehat{\mathbf{P} + \mathbf{p}}) \cdot \boldsymbol{\sigma}_i) (\hat{\mathbf{p}}) - \frac{1}{4} \frac{|\mathbf{P} - \mathbf{p}|}{|\mathbf{P} + \mathbf{p}|} I_4^P(\rho, |\mathbf{P} + \mathbf{p}|) ((\widehat{\mathbf{P} + \mathbf{p}}) \cdot \boldsymbol{\sigma}_i) (\widehat{\mathbf{P} - \mathbf{p}}) \right], \quad (\text{A9}) \end{aligned}$$

$$\begin{aligned} \mathbf{J}_{i,2b}^{\text{eff,ex}}(\hat{c}_6 \text{ term}) &= -\frac{g_A}{F_\pi^2} \frac{\tau_i^3}{2} \left(\frac{1 + \hat{c}_6}{4m} \right) \frac{4}{(2\pi)^3} \frac{1}{2} \left[\int_0^{k_F} \frac{\mathbf{p} \times (\boldsymbol{\sigma}_i \times \mathbf{k}_i^{\text{ex}} + i\mathbf{k}_i^{\text{ex}})}{m_\pi^2 + (\mathbf{k}_i^{\text{ex}})^2} d^3 \mathbf{p}_j + \int_0^{k_F} \frac{\mathbf{p} \times (\boldsymbol{\sigma}_i \times \mathbf{k}_j^{\text{ex}} - i\mathbf{k}_j^{\text{ex}})}{m_\pi^2 + (\mathbf{k}_j^{\text{ex}})^2} d^3 \mathbf{p}_j \right] \\ &= \frac{g_A \rho}{mF_\pi^2} \frac{\tau_i^3}{2} \frac{1 + \hat{c}_6}{4} \frac{1}{6} \left[\frac{I_{c_6}(\rho, |\mathbf{P} - \mathbf{p}|) \mathbf{p} \times (\boldsymbol{\sigma}_i \times (\mathbf{P} - \mathbf{p}))}{(\mathbf{P} - \mathbf{p})^2} - \frac{iI_{c_6}(\rho, |\mathbf{P} - \mathbf{p}|) \mathbf{p} \times \mathbf{P}}{(\mathbf{P} - \mathbf{p})^2} \right. \\ &\quad \left. - \frac{I_{c_6}(\rho, |\mathbf{P} + \mathbf{p}|) \mathbf{p} \times (\boldsymbol{\sigma}_i \times (\mathbf{P} + \mathbf{p}))}{(\mathbf{P} + \mathbf{p})^2} - \frac{iI_{c_6}(\rho, |\mathbf{P} + \mathbf{p}|) \mathbf{p} \times \mathbf{P}}{(\mathbf{P} + \mathbf{p})^2} \right], \quad (\text{A10}) \end{aligned}$$

where the integrals $I_1^\sigma(\rho, Q)$, $I_2^\sigma(\rho, Q)$, $I^P(\rho, Q)$, $I_{1,2,4}^P(\rho, Q)$, and $I_{c_6}(\rho, Q)$ are given by the following expressions

$$\begin{aligned} I_1^\sigma(\rho, Q) &= \frac{1}{k_F^3} \frac{9}{4} \int_0^{k_F} \int_{-1}^1 \frac{p^4(1 - \cos^2 \theta)}{m_\pi^2 + p^2 + \frac{Q^2}{4} - pQ \cos \theta} dp d \cos \theta \\ &= \frac{1}{512k_F^3 Q^3} \left(8k_F Q \left[48(k_F^2 + m_\pi^2)^2 + 32(k_F^2 - 3m_\pi^2)Q^2 - 3Q^4 \right] + 768m_\pi^3 Q^3 \operatorname{arccot} \left[\frac{m_\pi^2 + \frac{Q^2}{4} - k_F^2}{2m_\pi k_F} \right] \right. \\ &\quad \left. + 3 \left[16(k_F^2 + m_\pi^2)^2 - 8(k_F^2 - 5m_\pi^2)Q^2 + Q^4 \right] \left[4(k_F^2 + m_\pi^2) - Q^2 \right] \log \left[\frac{m_\pi^2 + (k_F - \frac{Q}{2})^2}{m_\pi^2 + (k_F + \frac{Q}{2})^2} \right] \right), \end{aligned} \quad (\text{A11})$$

$$\begin{aligned} I_2^\sigma(\rho, Q) &= \frac{1}{k_F^3} \frac{3}{2} \int_0^{k_F} \int_{-1}^1 \frac{p^4 + \frac{p^2 Q^2}{4} - p^3 Q \cos \theta}{m_\pi^2 + p^2 + \frac{Q^2}{4} - pQ \cos \theta} dp d \cos \theta \\ &= \frac{1}{16k_F^3 Q} \left(8k_F(2k_F^2 - 3m_\pi^2)Q + 24m_\pi^3 Q \operatorname{arccot} \left[\frac{m_\pi^2 + \frac{Q^2}{4} - k_F^2}{2m_\pi k_F} \right] + 3m_\pi^2 \left[4k_F^2 - Q^2 + 4m_\pi^2 \right] \log \left[\frac{m_\pi^2 + (k_F - \frac{Q}{2})^2}{m_\pi^2 + (k_F + \frac{Q}{2})^2} \right] \right), \end{aligned} \quad (\text{A12})$$

$$\begin{aligned} I^P(\rho, Q) &= \frac{1}{k_F^3} \frac{9}{8} \int_0^{k_F} \int_{-1}^1 \frac{p^4(6 \cos^2 \theta - 2) - 4p^3 Q \cos \theta + p^2 Q^2}{m_\pi^2 + p^2 + \frac{Q^2}{4} - pQ \cos \theta} dp d \cos \theta \\ &= -\frac{3}{512k_F^3 Q^3} \left(8k_F Q \left[48(k_F^2 + m_\pi^2)^2 - 32k_F^2 Q^2 - 3Q^4 \right] + 3 \left[4(k_F^2 + m_\pi^2) - Q^2 \right] \left[4m_\pi^2 + (2k_F - Q)^2 \right] \right. \\ &\quad \left. \times \left[4m_\pi^2 + (2k_F + Q)^2 \right] \log \left[\frac{m_\pi^2 + (k_F - \frac{Q}{2})^2}{m_\pi^2 + (k_F + \frac{Q}{2})^2} \right] \right), \end{aligned} \quad (\text{A13})$$

$$I_1^P(\rho, Q) = \frac{9}{4k_F^3} \int_0^{k_F} \int_{-1}^1 \frac{p^4(3 \cos^2 \theta - 1)}{m_\pi^2 + p^2 + \frac{Q^2}{4} - pQ \cos \theta} dp d \cos \theta,$$

$$I_2^P(\rho, Q) = \frac{9}{2k_F^3} \int_0^{k_F} \int_{-1}^1 \frac{p^3 Q \cos \theta}{m_\pi^2 + p^2 + \frac{Q^2}{4} - pQ \cos \theta} dp d \cos \theta,$$

$$I_4^P(\rho, Q) = \frac{9}{2k_F^3} \int_0^{k_F} \int_{-1}^1 \frac{p^2 Q^2}{m_\pi^2 + p^2 + \frac{Q^2}{4} - pQ \cos \theta} dp d \cos \theta,$$

$$I_1^P(\rho, Q) - I_2^P(\rho, Q) + \frac{1}{4} I_4^P(\rho, Q) = I^P(\rho, Q), \quad (\text{A14})$$

$$\begin{aligned} I_{c_6}(\rho, Q) &= \frac{9}{2k_F^3} \int_0^{k_F} \int_{-1}^1 \frac{\left(p^3 Q \cos \theta - \frac{p^2 Q^2}{2} \right)}{m_\pi^2 + p^2 + \frac{Q^2}{4} - pQ \cos \theta} dp d \cos \theta \\ &= -\frac{9}{128k_F^3 Q} \left(\left[32k_F^3 Q + 32k_F m_\pi^2 Q + 8k_F Q^3 \right] + \left[16(k_F^2 + m_\pi^2)^2 + 8(m_\pi^2 - k_F^2)Q^2 + Q^4 \right] \log \left[\frac{4m_\pi^2 + (2k_F - Q)^2}{4m_\pi^2 + (2k_F + Q)^2} \right] \right). \end{aligned} \quad (\text{A15})$$

Appendix B: Derivation of the structure factor $S_A(p)$

We start from the Lagrangian density for spin-dependent WIMP-nucleus scattering Eq. (1). WIMPs are expected to be nonrelativistic with velocities of the order $v/c \sim 10^{-3}$, so the time components of the currents can be neglected. Evaluating the Lagrangian density between initial and final states leads to

$$\langle f | \mathcal{L}_\chi^{\text{SD}} | i \rangle = -\frac{G_F}{\sqrt{2}} \int d^3 \mathbf{r} e^{-i\mathbf{p} \cdot \mathbf{r}} \bar{\chi}_f \boldsymbol{\gamma} \gamma_5 \chi_i \mathbf{J}_{fi}^A(\mathbf{r}), \quad (\text{B1})$$

where $e^{-i\mathbf{p}\cdot\mathbf{r}}\bar{\chi}_f\gamma\gamma^5\chi_i = \langle\chi_f|\mathbf{j}(\mathbf{r})|\chi_i\rangle$ represents the matrix element of the leptonic current of the WIMP and $\mathbf{J}_{fi}^A(\mathbf{r})$ that of the hadronic current.

We can expand the leptonic current in terms of spherical unit vectors [62]:

$$\bar{\chi}_f\gamma\gamma^5\chi_i e^{-i\mathbf{p}\cdot\mathbf{r}} = \mathbf{1} e^{-i\mathbf{p}\cdot\mathbf{r}} = \sum_{\lambda=0,\pm 1} l_\lambda \mathbf{e}_\lambda^\dagger e^{-i\mathbf{p}\cdot\mathbf{r}}, \quad (\text{B2})$$

with spherical unit vectors with a z -axis in the direction of \mathbf{p}

$$\mathbf{e}_{\pm 1} \equiv \mp \frac{1}{\sqrt{2}}(\mathbf{e}_{p1} \pm i\mathbf{e}_{p2}) \quad \mathbf{e}_0 \equiv \frac{\mathbf{p}}{|\mathbf{p}|}, \quad (\text{B3})$$

$$l_{\pm 1} = \mp \frac{1}{\sqrt{2}}(l_1 \pm il_2) \quad l_{\lambda=0} \equiv l_3. \quad (\text{B4})$$

We can also expand the product $\mathbf{e}_\lambda^\dagger e^{-i\mathbf{p}\cdot\mathbf{r}}$ in Eq. (B2) in a multipole expansion [62]. This leads to

$$\langle f|\mathcal{L}_\chi^{\text{SD}}|i\rangle = -\frac{G_F}{\sqrt{2}}\langle J_f M_f|\left(\sum_{L\geq 0}\sqrt{4\pi(2L+1)}(-i)^L l_3 \mathcal{L}_{L0}^5(p) - \sum_{L\geq 1}\sqrt{2\pi(2L+1)}(-i)^L \sum_{\lambda=\pm 1} l_\lambda [\mathcal{T}_{L-\lambda}^{\text{el}5}(p) + \lambda \mathcal{T}_{L-\lambda}^{\text{mag}5}(p)]\right)|J_i M_i\rangle, \quad (\text{B5})$$

where $|J_i M_i\rangle, |J_f M_f\rangle$ denote the initial and final states of the nucleus, $p = |\mathbf{p}|$. The electric longitudinal, electric transverse, and magnetic transverse multipole operators are defined by [62]

$$\mathcal{L}_{LM}^5(p) = \frac{i}{p} \int d^3\mathbf{r} [\nabla [j_L(pr)Y_{LM}(\Omega_r)]] \cdot \mathbf{J}^A(\mathbf{r}), \quad (\text{B6})$$

$$\mathcal{T}_{LM}^{\text{el}5}(p) = \frac{1}{p} \int d^3\mathbf{r} [\nabla \times j_L(pr)\mathbf{Y}_{LL1}^M(\Omega_r)] \cdot \mathbf{J}^A(\mathbf{r}), \quad (\text{B7})$$

$$\mathcal{T}_{LM}^{\text{mag}5}(p) = \int d^3\mathbf{r} [j_L(pr)\mathbf{Y}_{LL1}^M(\Omega_r)] \cdot \mathbf{J}^A(\mathbf{r}), \quad (\text{B8})$$

with spherical Bessel function $j_L(pr)$. The vector spherical harmonics are given by

$$\mathbf{Y}_{LL'1}^M(\Omega_r) = \sum_{m\lambda} \langle L'm1\lambda|L'1LM\rangle Y_{L'm}(\Omega_r) \mathbf{e}_\lambda. \quad (\text{B9})$$

Since $\mathbf{J}^A(\mathbf{r}) = \sum_{i=1}^A \mathbf{J}_i^A(\mathbf{r})\delta(\mathbf{r} - \mathbf{r}_i)$, the multipole operators can be written as a sum of one-body operators:

$$\begin{aligned} \mathcal{L}_{LM}^5(p) &= \frac{i}{p} \sum_{i=1}^A [\nabla [j_L(pr_i)Y_{LM}(\mathbf{r}_i)]] \cdot \mathbf{J}_i^A(\mathbf{r}_i) \\ &= \frac{i}{\sqrt{2L+1}} \sum_{i=1}^A [\sqrt{L+1}j_{L+1}(pr_i)\mathbf{Y}_{L(L+1)1}^M(\mathbf{r}_i) + \sqrt{L}j_{L-1}(pr_i)\mathbf{Y}_{L(L-1)1}^M(\mathbf{r}_i)] \cdot \mathbf{J}_i^A(\mathbf{r}_i), \end{aligned} \quad (\text{B10})$$

$$\begin{aligned} \mathcal{T}_{LM}^{\text{el}5}(p) &= \frac{1}{p} \sum_{i=1}^A [\nabla \times j_L(pr_i)\mathbf{Y}_{LL1}^M(\mathbf{r}_i)] \cdot \mathbf{J}_i^A(\mathbf{r}_i) \\ &= \frac{i}{\sqrt{2L+1}} \sum_{i=1}^A [\sqrt{L+1}j_{L-1}(pr_i)\mathbf{Y}_{L(L-1)1}^M(\mathbf{r}_i) - \sqrt{L}j_{L+1}(pr_i)\mathbf{Y}_{L(L+1)1}^M(\mathbf{r}_i)] \cdot \mathbf{J}_i^A(\mathbf{r}_i), \end{aligned} \quad (\text{B11})$$

$$\mathcal{T}_{LM}^{\text{mag}5}(p) = \sum_{i=1}^A j_L(pr_i)\mathbf{Y}_{LL1}^M(\mathbf{r}_i) \cdot \mathbf{J}_i^A(\mathbf{r}_i). \quad (\text{B12})$$

The structure factor $S_A(p)$ is obtained from $|\langle f|\mathcal{L}_\chi^{\text{SD}}|i\rangle|^2$ by summing over the final neutralino spin and over the nucleus final-state angular momentum projections, and by averaging over the initial configurations. It is thus useful to work with reduced matrix elements that do not depend on projection numbers:

$$\langle J_f M_f|O_{LM}|J_i M_i\rangle = (-1)^{J_f - M_f} \begin{pmatrix} J_f & L & J_i \\ -M_f & M & M_i \end{pmatrix} \langle J_f||O_L||J_i\rangle, \quad (\text{B13})$$

with $3j$ coefficients and where O is a tensor operator of rank L . This gives for the sum and average [62]

$$\begin{aligned} \frac{1}{2(2J_i+1)} \sum_{s_f, s_i} \sum_{M_f, M_i} |\langle f | \mathcal{L}_\chi^{\text{SD}} | i \rangle|^2 &= \frac{G_F^2}{4} \frac{1}{(2J_i+1)} \sum_{s_f, s_i} \left(\sum_{L \geq 0} 4\pi l_3 l_3^* |\langle J_f | \mathcal{L}_L^5 | J_i \rangle|^2 + \sum_{\lambda=\pm 1} l_\lambda l_\lambda^* \sum_{L \geq 1} 2\pi |\langle J_f | \mathcal{T}_L^{\text{el5}} + \lambda \mathcal{T}_L^{\text{mag5}} | J_i \rangle|^2 \right) \\ &= \frac{G_F^2}{4} \frac{4\pi}{(2J_i+1)} \sum_{s_f, s_i} \left(\sum_{L \geq 0} l_3 l_3^* |\langle J_f | \mathcal{L}_L^5 | J_i \rangle|^2 + \sum_{L \geq 1} \left[\frac{1}{2} (\mathbf{1} \cdot \mathbf{1}^* - l_3 l_3^*) \left(|\langle J_f | \mathcal{T}_L^{\text{el5}} | J_i \rangle|^2 \right. \right. \right. \\ &\quad \left. \left. \left. + |\langle J_f | \mathcal{T}_L^{\text{mag5}} | J_i \rangle|^2 \right) - \frac{i}{2} (\mathbf{1} \times \mathbf{1}^*)_3 \left(2 \text{Re} \langle J_f | \mathcal{T}_L^{\text{el5}} | J_i \rangle \langle J_f | \mathcal{T}_L^{\text{mag5}} | J_i \rangle^* \right) \right] \right), \end{aligned} \quad (\text{B14})$$

where we have assumed that the neutralino spin is $1/2$, and the cross terms vanish due to the orthogonalization properties of the $3j$ coefficients. For the sum over neutralino spin projections one has for $\mu, \nu = 1, 2, 3$

$$\begin{aligned} - \sum_{s_i, s_f} l_\mu l_\nu^* &= \sum_{s_i, s_f} \bar{\chi}^{s_f}(p_f) \gamma^\mu \gamma^5 \chi^{s_i}(p_i) \bar{\chi}^{s_i}(p_i) \gamma^5 \gamma^\nu \chi^{s_f}(p_f), \\ &= \sum_{s_i, s_f} (\chi_\delta^{s_f}(p_f) \bar{\chi}_\alpha^{s_f}(p_f) (\gamma^\mu \gamma^5)_{\alpha\beta} \chi_\beta^{s_i}(p_i) \bar{\chi}_\gamma^{s_i}(p_i) (\gamma^5 \gamma^\nu)_{\gamma\delta}), \\ &= \frac{1}{4} [2\text{Tr}(\gamma^0 \gamma^\mu \gamma^5 \gamma^5 \gamma^\nu) + 2\text{Tr}(\gamma^\mu \gamma^5 \gamma^5 \gamma^\nu)] = \frac{1}{2} \text{Tr}(\gamma^\mu \gamma^5 \gamma^5 \gamma^\nu) = -2\delta^{\mu\nu}, \end{aligned} \quad (\text{B15})$$

which follows from the completeness relation

$$\sum_s \chi_\alpha^s(p) \bar{\chi}_\beta^s(p) = \left(\frac{p_\mu \gamma^\mu + m}{2E_p} \right)_{\alpha\beta} \approx \frac{1}{2} (\gamma^0 + \mathbf{1})_{\alpha\beta}, \quad (\text{B16})$$

valid for nonrelativistic WIMPs. Combined, this gives the final result:

$$\frac{1}{2(2J_i+1)} \sum_{s_f, s_i} \sum_{M_f, M_i} |\langle f | \mathcal{L}_\chi^{\text{SD}} | i \rangle|^2 = \frac{G_F^2}{2} \frac{4\pi}{(2J_i+1)} \left[\sum_{L \geq 0} |\langle J_f | \mathcal{L}_L^5 | J_i \rangle|^2 + \sum_{L \geq 1} \left(|\langle J_f | \mathcal{T}_L^{\text{el5}} | J_i \rangle|^2 + |\langle J_f | \mathcal{T}_L^{\text{mag5}} | J_i \rangle|^2 \right) \right]. \quad (\text{B17})$$

The specific form of the multipoles depends on the form of the WIMP currents $\mathbf{J}_i^A(\mathbf{r})$. They contain either axial-vector terms $[\boldsymbol{\sigma}_i]$ or pseudo-scalar ones $[(\mathbf{p} \cdot \boldsymbol{\sigma}_i)\mathbf{p}]$. For axial-vector currents, the response will be proportional to the following operator

$$\begin{aligned} M_{L,L'}^M(p\mathbf{r}_i) &= j_{L'}(pr_i) \mathbf{Y}_{LL1}^M(\mathbf{r}_i) \cdot \boldsymbol{\sigma}_i, \\ &= j_{L'}(pr_i) \sum_{m\lambda} \langle L'm1\lambda | L'1LM \rangle Y_{L'm}(\mathbf{r}_i) \sigma_i^{1\lambda} = j_{L'}(pr_i) [Y_{L'}(\mathbf{r}_i) \boldsymbol{\sigma}_i]^L. \end{aligned} \quad (\text{B18})$$

Pseudo-Scalar currents, which are proportional to the momentum transfer \mathbf{p} , only contribute to the longitudinal multipoles (see Eq. (B5)). Moreover, in these we can replace $(\mathbf{p} \cdot \boldsymbol{\sigma}_i)\mathbf{p}$ by $p^2 \boldsymbol{\sigma}_i$, because of

$$(\mathbf{p} \cdot \boldsymbol{\sigma}_i)\mathbf{p} = p^2 \boldsymbol{\sigma}_i + \mathbf{p} \times (\mathbf{p} \times \boldsymbol{\sigma}_i), \quad (\text{B19})$$

and the second term is perpendicular to \mathbf{p} , so it vanishes for the longitudinal multipoles. As a result, pseudo-scalar currents can also be expressed in terms of $M_{L,L'}^M(p\mathbf{r}_i)$.

In summary, including chiral 2b currents at the normal-ordered one-body level in Eq. (19), we have for the multipoles

$$\begin{aligned} \mathcal{L}_L^5(p) &= \frac{i}{\sqrt{2L+1}} \sum_{i=1}^A \frac{1}{2} \left[a_0 + a_1 \tau_i^3 \left(1 + \delta a_1(p) - \frac{2g_{\pi p m} F_\pi p^2}{2mg_A(p^2 + m_\pi^2)} + \delta a_1^P(p) \right) \right] \\ &\quad \times \left[\sqrt{L+1} M_{L,L+1}(p\mathbf{r}_i) + \sqrt{L} M_{L,L-1}(p\mathbf{r}_i) \right], \end{aligned} \quad (\text{B20})$$

$$\mathcal{T}_L^{\text{el5}}(p) = \frac{i}{\sqrt{2L+1}} \sum_{i=1}^A \frac{1}{2} \left[a_0 + a_1 \tau_i^3 \left(1 - 2 \frac{p^2}{\Lambda_A^2} + \delta a_1(p) \right) \right] \left[-\sqrt{L} M_{L,L+1}(p\mathbf{r}_i) + \sqrt{L+1} M_{L,L-1}(p\mathbf{r}_i) \right], \quad (\text{B21})$$

$$\mathcal{T}_L^{\text{mag5}}(p) = \sum_{i=1}^A \frac{1}{2} \left[a_0 + a_1 \tau_i^3 \left(1 - 2 \frac{p^2}{\Lambda_A^2} + \delta a_1(p) \right) \right] M_{L,L}(p\mathbf{r}_i). \quad (\text{B22})$$

Note that the p^2/Λ_A^2 terms cancel in the longitudinal response and only contribute to the transverse multipoles.

Appendix C: Reduced matrix elements of $M_{L,L'}(pr_i)$

To calculate the structure factor, we need the matrix elements of the one-body operator $M_{L,L'}(pr_i) = j_{L'}(pr_i) \times [Y_{L'}(\hat{\mathbf{r}}_i) \boldsymbol{\sigma}_i]^L$ between the single-particle states of the many-body basis used for the description of the nuclear states. The reduced matrix elements can be obtained as a function of $3j$ and $9j$ symbols and matrix elements of the spherical Bessel functions $j_{L'}$,

$$\begin{aligned}
& \langle n'l' \frac{1}{2} j' || M_{L,L'}(pr_i) || n l \frac{1}{2} j \rangle \\
&= \sum_{n''l''} \langle n'l' || j_{L'} Y_{L'} || n''l'' \rangle \langle n''l'' \frac{1}{2} || \boldsymbol{\sigma}_i || n l \frac{1}{2} \rangle [(2j+1)(2j'+1)(2L+1)]^{\frac{1}{2}} \left\{ \begin{matrix} l' & l & L' \\ \frac{1}{2} & \frac{1}{2} & 1 \\ j' & j & L \end{matrix} \right\} \\
&= \langle n'l' | j_{L'} | nl \rangle \langle n'l' | Y_{L'} | nl \rangle \langle \frac{1}{2} || \boldsymbol{\sigma}_i || \frac{1}{2} \rangle [(2j+1)(2j'+1)(2L+1)]^{\frac{1}{2}} \left\{ \begin{matrix} l' & l & L' \\ \frac{1}{2} & \frac{1}{2} & 1 \\ j' & j & L \end{matrix} \right\} \\
&= \langle n'l' | j_{L'}(pr_i) | nl \rangle (-1)^{l'} \sqrt{\frac{6}{4\pi}} [(2l'+1)(2l+1)(2j'+1)(2j+1)]^{\frac{1}{2}} [(2L'+1)(2L+1)]^{\frac{1}{2}} \\
&\quad \times \begin{pmatrix} l' & L' & l \\ 0 & 0 & 0 \end{pmatrix} \left\{ \begin{matrix} l' & l & L' \\ \frac{1}{2} & \frac{1}{2} & 1 \\ j' & j & L \end{matrix} \right\}. \tag{C1}
\end{aligned}$$

Appendix D: Fits of the structure factors

In Tables IV-VIII we give fits for the isoscalar/isovector and “neutron-only” / “proton-only” decompositions of the structure factors of all isotopes studied in this work. Results are given including 1b+2b currents.

-
- [1] R. J. Gaitskell, *Annu. Rev. Nucl. Part. Sci.* **54**, 315 (2004).
- [2] G. Bertone, D. Hooper, and J. Silk, *Phys. Rep.* **405**, 279 (2005).
- [3] J. L. Feng, *Annu. Rev. Astron. Astrophys.* **48**, 495 (2010).
- [4] L. Baudis, *Phys. Dark Univ.* **1**, 94 (2012).
- [5] J. Engel, S. Pittel, and P. Vogel, *Int. J. Mod. Phys. E* **01**, 1 (1992).
- [6] J. Angle *et al.* (XENON10 Collaboration), *Phys. Rev. Lett.* **101**, 091301 (2008).
- [7] V. N. Lebedenko *et al.* (ZEPLIN-III Collaboration), *Phys. Rev. Lett.* **103**, 151302 (2009).
- [8] E. Behnke *et al.* (COUPP Collaboration), *Phys. Rev. Lett.* **106**, 021303 (2011).
- [9] S. Archambault *et al.* (PICASSO Collaboration), *Phys. Lett. B* **711**, 153 (2012).
- [10] S. Kim *et al.* (KIMS Collaboration), *Phys. Rev. Lett.* **108**, 181301 (2012).
- [11] M. Felizardo *et al.* (SIMPLE Collaboration), *Phys. Rev. Lett.* **108**, 201302 (2012).
- [12] E. Aprile *et al.* (XENON100 Collaboration), *Phys. Rev. Lett.* **111**, 021301 (2013).
- [13] A. L. Fitzpatrick, W. C. Haxton, E. Katz, N. Lubbers, and Y. Xu, *JCAP* **1302**, 004 (2013).
- [14] V. Cirigliano, M. L. Graesser, and G. Ovanessian, *JHEP* **1210**, 025 (2012).
- [15] J. Menéndez, D. Gazit, and A. Schwenk, *Phys. Rev. D* **86**, 103511 (2012).
- [16] A. L. Fitzpatrick, W. C. Haxton, E. Katz, N. Lubbers, and Y. Xu, arXiv:1211.2818.
- [17] M. T. Ressell, M. B. Aufderheide, S. D. Bloom, K. Griest, G. J. Mathews, and D. A. Resler, *Phys. Rev. D* **48**, 5519 (1993).
- [18] J. Engel, M. T. Ressell, I. S. Towner, and W. E. Ormand, *Phys. Rev. C* **52**, 2216 (1995).
- [19] V. I. Dimitrov, J. Engel, and S. Pittel, *Phys. Rev. D* **51**, R291 (1995).
- [20] M. T. Ressell and D. J. Dean, *Phys. Rev. C* **56**, 535 (1997).
- [21] P. C. Divari, T. S. Kosmas, J. D. Vergados, and L. D. Skouras, *Phys. Rev. C* **61**, 054612 (2000).
- [22] M. Kortelainen, T. S. Kosmas, J. Suhonen, and J. Toivanen, *Phys. Lett. B* **632**, 226 (2006).
- [23] P. Toivanen, M. Kortelainen, J. Suhonen, and J. Toivanen, *Phys. Rev. C* **79**, 044302 (2009).
- [24] E. Epelbaum, H.-W. Hammer, and U.-G. Meißner, *Rev. Mod. Phys.* **81**, 1773 (2009).
- [25] H.-W. Hammer, A. Nogga, and A. Schwenk, *Rev. Mod. Phys.* **85**, 197 (2013).
- [26] E. Aprile *et al.* (XENON100 Collaboration), *Phys. Rev. Lett.* **109**, 181301 (2012).
- [27] D. G. Cerdeño, M. Fornasa, J. H. Huh, and M. Peiró, *Phys. Rev. D* **87**, 023512 (2013).
- [28] M. Butler, J.-W. Chen, and X. Kong, *Phys. Rev. C* **63**, 035501 (2001).
- [29] S. Nakamura, T. Sato, V. P. Gudkov, and K. Kubodera, *Phys. Rev. C* **63**, 034617 (2001).
- [30] D. Gazit, *Electro-Weak Interactions in Light Nuclei* (Ph.D. Thesis, Hebrew University of Jerusalem, 2007), arXiv:0807.0216.
- [31] D. Gazit and N. Barnea, *Phys. Rev. Lett.* **98**, 192501 (2007).
- [32] E. O'Connor, D. Gazit, C. J. Horowitz, A. Schwenk, and N. Barnea, *Phys. Rev. C* **75**, 055803 (2007).
- [33] A. Arcones, G. Martínez-Pinedo, E. O'Connor, A. Schwenk, H.-T. Janka, C. J. Horowitz, and K. Langanke, *Phys. Rev. C* **78**, 015806 (2008).
- [34] J. Menéndez, D. Gazit, and A. Schwenk, *Phys. Rev. Lett.* **107**, 062501 (2011).
- [35] M. Cannoni, *Phys. Rev. D* **87**, 075014 (2013).
- [36] P. C. Divari, and J. D. Vergados, arXiv:1301.1457.
- [37] G. Jungman, M. Kamionkowski, and K. Griest, *Phys. Rep.* **267**, 195 (1996).
- [38] V. Bernard, L. Elouadrhiri, and U.-G. Meißner, *J. Phys. G* **28**, R1 (2002).
- [39] C. E. Carlson and J. L. Poor, *Phys. Rev. D* **36**, 2169 (1987).
- [40] T. S. Park, L. E. Marcucci, R. Schiavilla, M. Viviani, A. Kievsky, S. Rosati, K. Kubodera, D.-P. Min, and M. Rho, *Phys. Rev. C* **67**, 055206 (2003).
- [41] B. Friman and A. Schwenk, in *From Nuclei to Stars*, Festschrift in Honor of Gerald E. Brown, edited by S. Lee (World Scientific, Singapore, 2011), arXiv:1101.4858.
- [42] J. W. Holt, N. Kaiser, and W. Weise, *Phys. Rev. C* **79**, 054331 (2009); *ibid.* **81**, 024002 (2010).
- [43] D. R. Entem and R. Machleidt, *Phys. Rev. C* **68**, 041001(R) (2003).
- [44] E. Epelbaum, W. Glöckle, and U.-G. Meißner, *Nucl. Phys. A* **747**, 362 (2005).
- [45] M. C. M. Rentmeester, R. G. E. Timmermans, and J. J. de Swart, *Phys. Rev. C* **67**, 044001 (2003).
- [46] V. Bernard, N. Kaiser, and U.-G. Meißner *Nucl. Phys. A* **615**, 483 (1997).
- [47] E. Caurier, G. Martínez-Pinedo, F. Nowacki, A. Poves, and A. P. Zuker, *Rev. Mod. Phys.* **77**, 427 (2005).
- [48] E. Caurier, J. Menéndez, F. Nowacki, and A. Poves, *Phys. Rev. Lett.* **100**, 052503 (2008).
- [49] J. Menéndez, A. Poves, E. Caurier, and F. Nowacki, *Nucl. Phys. A* **818**, 139 (2009).
- [50] K. Sieja, G. Martínez-Pinedo, L. Coquard, and N. Pietralla, *Phys. Rev. C* **80**, 054311 (2009).
- [51] E. Caurier, F. Nowacki, A. Poves, and K. Sieja, *Phys. Rev. C* **82**, 064304 (2010).
- [52] J. Menéndez, A. Poves, E. Caurier, and F. Nowacki, *Phys. Rev. C* **80**, 048501 (2009).
- [53] Q. Zhi, K. Langanke, G. Martínez-Pinedo, F. Nowacki, and K. Sieja, *Nucl. Phys. A* **859**, 172 (2011).
- [54] B. A. Brown and B. H. Wildenthal, *Annu. Rev. Nucl. Part. Sci.* **38**, 29 (1988).
- [55] B. A. Brown and W. A. Richter, *Phys. Rev. C* **74**, 034315 (2006).
- [56] T. Otsuka, T. Suzuki, J. D. Holt, A. Schwenk, and Y. Akaishi, *Phys. Rev. Lett.* **105**, 032501 (2010).
- [57] J. D. Holt, T. Otsuka, A. Schwenk, and T. Suzuki, *J. Phys. G* **39**, 085111 (2012).
- [58] A. T. Gallant *et al.*, *Phys. Rev. Lett.* **109**, 032506 (2012).
- [59] F. Wienholtz *et al.*, *Nature* **498**, 346 (2013).
- [60] J. D. Holt, J. Menéndez, and A. Schwenk, *Phys. Rev. Lett.* **110**, 022502 (2013).
- [61] J. D. Holt, J. Menéndez, and A. Schwenk, *Eur. Phys. J. A* **49**, 39 (2013).

- [62] J. D. Walecka, *Theoretical Nuclear and Subnuclear Physics* (Oxford University Press, New York, 1995).

TABLE IV. Fits to the isoscalar/isovector structure factors S_{00} , S_{11} and S_{01} as well as “proton-only” and “neutron-only” structure factors S_p and S_n for spin-dependent WIMP elastic scattering off ^{129}Xe and ^{131}Xe nuclei, including 1b and 2b currents as in Fig. 6. The upper and lower limits from the theoretical error band were used for the fit. The fitting function of the dimensionless variable $u = p^2 b^2/2$ is $S_{ij}(u) = e^{-u} \sum_{n=0}^9 c_{ij,n} u^n$. The rows give the coefficients $c_{ij,n}$ of the u^n terms in the polynomial.

^{129}Xe					
$u = p^2 b^2/2, b = 2.2853 \text{ fm}$					
$e^{-u} \times$	S_{00}	$S_{11} (1b+2b \text{ min})$	$S_{11} (1b+2b \text{ max})$	$S_{01} (1b+2b \text{ min})$	$S_{01} (1b+2b \text{ max})$
1	0.0547144	0.0221559	0.0357742	-0.0885644	-0.0696691
u	-0.146407	-0.0656100	-0.107895	0.254049	0.197380
u^2	0.180603	0.0863920	0.145055	-0.332322	-0.254839
u^3	-0.125526	-0.0631729	-0.108549	0.244981	0.185896
u^4	0.0521484	0.0278792	0.0490401	-0.109298	-0.0825294
u^5	-0.0126363	-0.00756661	-0.0136169	0.0296705	0.0224322
u^6	0.00176284	0.00126767	0.00233283	-0.00492657	-0.00375109
u^7	-1.32501×10^{-4}	-1.27755×10^{-4}	-2.39926×10^{-4}	4.88467×10^{-4}	3.77179×10^{-4}
u^8	4.23423×10^{-6}	7.10322×10^{-6}	1.35553×10^{-5}	-2.65022×10^{-5}	-2.09510×10^{-5}
u^9	-1.68052×10^{-9}	-1.67272×10^{-7}	-3.21404×10^{-7}	5.98909×10^{-7}	4.92362×10^{-7}
$e^{-u} \times$		$S_p (1b+2b \text{ min})$	$S_p (1b+2b \text{ max})$	$S_n (1b+2b \text{ min})$	$S_n (1b+2b \text{ max})$
1		0.00196369	0.00715281	0.146535	0.179056
u		-0.00119154	-0.0134790	-0.409290	-0.508334
u^2		-0.00324210	0.00788823	0.521423	0.657560
u^3		0.00622602	0.00311153	-0.374011	-0.477988
u^4		-0.00496653	-0.00653771	0.162155	0.209437
u^5		0.00224469	0.00375478	-0.0424842	-0.0554186
u^6		-5.74412×10^{-4}	-0.00105558	0.00674911	0.00889251
u^7		8.31313×10^{-5}	1.59440×10^{-4}	-6.33434×10^{-4}	-8.42977×10^{-4}
u^8		-6.41114×10^{-6}	-1.25055×10^{-5}	3.20266×10^{-5}	4.30517×10^{-5}
u^9		2.07744×10^{-7}	4.04987×10^{-7}	-6.54245×10^{-7}	-8.88774×10^{-7}
^{131}Xe					
$u = p^2 b^2/2, b = 2.2905 \text{ fm}$					
$e^{-u} \times$	S_{00}	$S_{11} (1b+2b \text{ min})$	$S_{11} (1b+2b \text{ max})$	$S_{01} (1b+2b \text{ min})$	$S_{01} (1b+2b \text{ max})$
1	0.0417857	0.0167361	0.0271052	-0.0675438	-0.0529487
u	-0.111132	-0.0472853	-0.0812985	0.195710	0.146987
u^2	0.171306	0.0684924	0.122960	-0.306688	-0.225003
u^3	-0.132481	-0.0514413	-0.0940491	0.243678	0.179499
u^4	0.0630161	0.0237858	0.0439746	-0.118395	-0.0888278
u^5	-0.0177684	-0.00692778	-0.0128013	0.0351428	0.0271514
u^6	0.00282192	0.00124370	0.00227407	-0.00622577	-0.00499280
u^7	-2.32247×10^{-4}	-1.31617×10^{-4}	-2.35642×10^{-4}	6.31685×10^{-4}	5.31148×10^{-4}
u^8	7.81471×10^{-6}	7.46669×10^{-6}	1.28691×10^{-5}	-3.33272×10^{-5}	-2.99162×10^{-5}
u^9	1.25984×10^{-9}	-1.73484×10^{-7}	-2.77011×10^{-7}	6.82500×10^{-7}	6.81902×10^{-7}
$e^{-u} \times$		$S_p (1b+2b \text{ min})$	$S_p (1b+2b \text{ max})$	$S_n (1b+2b \text{ min})$	$S_n (1b+2b \text{ max})$
1		0.00159352	0.00529643	0.111627	0.136735
u		-0.00207344	-0.00528808	-0.308602	-0.393930
u^2		0.00567412	-0.00627452	0.474842	0.617924
u^3		-0.00605643	0.0227436	-0.375201	-0.488443
u^4		0.00337794	-0.0192229	0.182382	0.234645
u^5		-6.88135×10^{-4}	0.00844826	-0.0539711	-0.0681357
u^6		-3.42717×10^{-5}	-0.00212755	0.00944180	0.0116393
u^7		3.13222×10^{-5}	3.03972×10^{-4}	-9.34456×10^{-4}	-0.00111487
u^8		-4.02617×10^{-6}	-2.27893×10^{-5}	4.73386×10^{-5}	5.34878×10^{-5}
u^9		1.72711×10^{-7}	7.05661×10^{-7}	-9.01514×10^{-7}	-9.03594×10^{-7}

TABLE V. Fits to the isoscalar/isovector structure factors S_{00} , S_{11} and S_{01} as well as “proton-only” and “neutron-only” structure factors S_p and S_n for spin-dependent WIMP elastic scattering off ^{73}Ge (Int. 2) and ^{127}I nuclei, including 1b and 2b currents as in Fig. 10 and Fig. 11. The upper and lower limits from the theoretical error band were used for the fit. The fitting function of the dimensionless variable $u = p^2 b^2 / 2$ is $S_{ij}(u) = e^{-u} \sum_{n=0}^9 c_{ij,n} u^n$. The rows give the coefficients $c_{ij,n}$ of the u^n terms in the polynomial.

^{73}Ge (Int.2)					
$u = p^2 b^2 / 2, b = 2.1058 \text{ fm}$					
$e^{-u} \times$	S_{00}	S_{11} (1b+2b min)	S_{11} (1b+2b max)	S_{01} (1b+2b min)	S_{01} (1b+2b max)
1	0.215608	0.0743728	0.120045	-0.321836	-0.253289
u	-0.578786	-0.233814	-0.384157	0.950136	0.739394
u^2	0.698020	0.341725	0.559728	-1.27413	-0.993188
u^3	-0.372000	-0.259024	-0.415686	0.831035	0.659953
u^4	0.107576	0.121206	0.188412	-0.323769	-0.269522
u^5	-0.0182408	-0.0371226	-0.0568025	0.0831244	0.0745897
u^6	0.00217108	0.00741080	0.0120204	-0.0151542	-0.0144162
u^7	-2.07981×10^{-4}	-9.02610×10^{-4}	-0.00175855	0.00193259	0.00181542
u^8	1.65907×10^{-5}	5.81933×10^{-5}	1.59975×10^{-4}	-1.55025×10^{-4}	-1.29365×10^{-4}
u^9	-5.95664×10^{-7}	-1.38557×10^{-6}	-6.66472×10^{-6}	5.68777×10^{-6}	3.77020×10^{-6}
$e^{-u} \times$		S_p (1b+2b min)	S_p (1b+2b max)	S_n (1b+2b min)	S_n (1b+2b max)
1		0.0138433	0.0366954	0.543270	0.657509
u		-0.0138982	-0.0733258	-1.55198	-1.91400
u^2		-0.00961825	0.0471313	2.03269	2.53820
u^3		0.0275620	0.0281229	-1.28990	-1.63488
u^4		-0.0101577	-0.0405538	0.496419	0.639763
u^5		-0.00235492	0.0196085	-0.128347	-0.171656
u^6		0.00246030	-0.00515247	0.0232676	0.0345442
u^7		-6.53041×10^{-4}	8.06626×10^{-4}	-0.00274482	-0.00504185
u^8		7.84526×10^{-5}	-6.95571×10^{-5}	1.81026×10^{-4}	4.64828×10^{-4}
u^9		-3.61078×10^{-6}	2.63102×10^{-6}	-4.56383×10^{-6}	-1.93402×10^{-5}
^{127}I					
$u = p^2 b^2 / 2, b = 2.2801 \text{ fm}$					
$e^{-u} \times$	S_{00}	S_{11} (1b+2b min)	S_{11} (1b+2b max)	S_{01} (1b+2b min)	S_{01} (1b+2b max)
1	0.0928480	0.0297755	0.0480576	0.105154	0.133610
u	-0.252496	-0.0904582	-0.148155	-0.302437	-0.388379
u^2	0.351982	0.145234	0.234436	0.452142	0.579490
u^3	-0.260427	-0.132020	-0.205618	-0.371193	-0.471030
u^4	0.118280	0.0769978	0.113448	0.192342	0.238903
u^5	-0.0319614	-0.0290350	-0.0396327	-0.0631442	-0.0751672
u^6	0.00492618	0.00701812	0.00870215	0.0130940	0.0144759
u^7	-4.06546×10^{-4}	-0.00105740	-0.00116942	-0.00169645	-0.00166889
u^8	1.55818×10^{-5}	9.11013×10^{-5}	8.85742×10^{-5}	1.28905×10^{-4}	1.07845×10^{-4}
u^9	-1.64934×10^{-7}	-3.44003×10^{-6}	-2.91582×10^{-6}	-4.47150×10^{-6}	-3.09335×10^{-6}
$e^{-u} \times$		S_p (1b+2b min)	S_p (1b+2b max)	S_n (1b+2b min)	S_n (1b+2b max)
1		0.227779	0.274511	0.00729876	0.0174634
u		-0.645502	-0.788708	-0.0124606	-0.0401552
u^2		0.950398	1.16333	0.00820860	0.0429504
u^3		-0.766815	-0.929643	0.00187492	-0.0171587
u^4		0.391958	0.460285	-0.00353024	-5.50598×10^{-4}
u^5		-0.127209	-0.138933	0.00121496	0.00367288
u^6		0.0262471	0.0247388	5.05292×10^{-5}	-0.00150561
u^7		-0.00342824	-0.00242940	-1.09891×10^{-4}	2.73729×10^{-4}
u^8		2.66810×10^{-4}	1.08740×10^{-4}	2.14196×10^{-5}	-2.38605×10^{-5}
u^9		-9.56532×10^{-6}	-8.75631×10^{-7}	-1.29204×10^{-6}	8.31918×10^{-7}

TABLE VI. Fits to the isoscalar/isovector structure factors S_{00} , S_{11} and S_{01} as well as “proton-only” and “neutron-only” structure factors S_p and S_n for spin-dependent WIMP elastic scattering off ^{19}F , including 1b and 2b currents as in Fig. 12. The upper and lower limits from the theoretical error band were used for the fit. The fitting function of the dimensionless variable $u = p^2 b^2 / 2$ is $S_{ij}(u) = e^{-u} \sum_{n=0}^{14} c_{ij,n} u^n$. The rows give the coefficients $c_{ij,n}$ of the u^n terms in the polynomial.

^{19}F					
$u = p^2 b^2 / 2, b = 1.8032 \text{ fm}$					
$e^{-u} \times$	S_{00}	$S_{11} (1b+2b \text{ min})$	$S_{11} (1b+2b \text{ max})$	$S_{01} (1b+2b \text{ min})$	$S_{01} (1b+2b \text{ max})$
1	0.108058	0.0505180	0.0815382	0.147769	0.187748
u	-0.143789	-0.102657	-0.172679	-0.248324	-0.324839
u^2	0.0680848	0.111644	0.212269	0.196804	0.292189
u^3	4.07415×10^{-4}	-0.103800	-0.228208	-0.110517	-0.243481
u^4	-0.0314817	0.0920875	0.213050	0.0431978	0.225724
u^5	0.0385933	-0.0693892	-0.153539	0.00355133	-0.187879
u^6	-0.0293716	0.0406756	0.0811970	-0.0214773	0.120370
u^7	0.0152264	-0.0180247	-0.0312282	0.0171137	-0.0567987
u^8	-0.00552655	0.00597662	0.00872716	-0.00777410	0.0195241
u^9	0.00141965	-0.00146688	-0.00176305	0.00231495	-0.00485435
u^{10}	-2.56989×10^{-4}	2.61654×10^{-4}	2.53666×10^{-4}	-4.67535×10^{-4}	8.61430×10^{-4}
u^{11}	3.20688×10^{-5}	-3.28624×10^{-5}	-2.52190×10^{-5}	6.36451×10^{-5}	-1.06203×10^{-4}
u^{12}	-2.62562×10^{-6}	2.74752×10^{-6}	1.63658×10^{-6}	-5.60211×10^{-6}	8.63415×10^{-6}
u^{13}	1.26950×10^{-7}	-1.36980×10^{-7}	-6.18772×10^{-8}	2.88239×10^{-7}	-4.15920×10^{-7}
u^{14}	-2.74719×10^{-9}	3.07589×10^{-9}	1.02158×10^{-9}	-6.58792×10^{-9}	8.98798×10^{-9}
$e^{-u} \times$		$S_p (1b+2b \text{ min})$	$S_p (1b+2b \text{ max})$	$S_n (1b+2b \text{ min})$	$S_n (1b+2b \text{ max})$
1		0.306344	0.377350	0.00186788	0.0108048
u		-0.494703	-0.641645	0.00680710	0.00209733
u^2		0.375778	0.575714	0.00639787	-0.0195694
u^3		-0.210605	-0.482204	-0.0611310	0.0180694
u^4		0.0963209	0.426127	0.114287	-0.00732843
u^5		-0.0171498	-0.322095	-0.118072	-0.00123149
u^6		-0.0189635	0.185010	0.0795624	0.00434979
u^7		0.0194977	-0.0786211	-0.0371512	-0.00349429
u^8		-0.00944981	0.0245769	0.0123395	0.00167052
u^9		0.00288142	-0.00561387	-0.00293887	-5.31956×10^{-4}
u^{10}		-5.87122×10^{-4}	9.23589×10^{-4}	4.98543×10^{-4}	1.15596×10^{-4}
u^{11}		8.01160×10^{-5}	-1.06384×10^{-4}	-5.88110×10^{-5}	-1.69465×10^{-5}
u^{12}		-7.04748×10^{-6}	8.13277×10^{-6}	4.58527×10^{-6}	1.60329×10^{-6}
u^{13}		3.61875×10^{-7}	-3.70365×10^{-7}	-2.12430×10^{-7}	-8.83654×10^{-8}
u^{14}		-8.24953×10^{-9}	7.60000×10^{-9}	4.42852×10^{-9}	2.15466×10^{-9}

TABLE VII. Fits to the isoscalar/isovector structure factors S_{00} , S_{11} and S_{01} as well as “proton-only” and “neutron-only” structure factors S_p and S_n for spin-dependent WIMP elastic scattering off ^{23}Na and ^{27}Al nuclei, including 1b and 2b currents as in Fig. 13. The upper and lower limits from the theoretical error band were used for the fit. The fitting function of the dimensionless variable $u = p^2 b^2/2$ is $S_{ij}(u) = e^{-u} \sum_{n=0}^9 c_{ij,n} u^n$. The rows give the coefficients $c_{ij,n}$ of the u^n terms in the polynomial.

^{23}Na					
$u = p^2 b^2/2, b = 1.8032 \text{ fm}$					
$e^{-u} \times$	S_{00}	$S_{11} (1b+2b \text{ min})$	$S_{11} (1b+2b \text{ max})$	$S_{01} (1b+2b \text{ min})$	$S_{01} (1b+2b \text{ max})$
1	0.0325305	0.00973487	0.0157138	0.0356077	0.0453141
u	-0.0433531	-0.0185306	-0.0312138	-0.0582455	-0.0772792
u^2	0.0319487	0.0199627	0.0351984	0.0551609	0.0769308
u^3	-0.00568858	-0.00905267	-0.0180647	-0.0210939	-0.0327180
u^4	2.67783×10^{-4}	0.00207003	0.00580816	0.00499454	0.00946296
u^5	2.44643×10^{-5}	-2.28653×10^{-4}	-0.00122900	-9.09266×10^{-4}	-0.00199807
u^6	-4.79620×10^{-6}	4.31460×10^{-6}	1.72086×10^{-4}	1.28051×10^{-4}	2.89585×10^{-4}
u^7	5.39846×10^{-7}	1.67535×10^{-6}	-1.52834×10^{-5}	-1.20016×10^{-5}	-2.59681×10^{-5}
u^8	-3.24691×10^{-8}	-1.67911×10^{-7}	7.73042×10^{-7}	6.29181×10^{-7}	1.25857×10^{-6}
u^9	8.09358×10^{-10}	5.14559×10^{-9}	-1.67756×10^{-8}	-1.39823×10^{-8}	-2.47908×10^{-8}
$e^{-u} \times$		$S_p (1b+2b \text{ min})$	$S_p (1b+2b \text{ max})$	$S_n (1b+2b \text{ min})$	$S_n (1b+2b \text{ max})$
1		0.0778747	0.0935155	0.00295139	0.00674243
u		-0.120203	-0.151102	0.00244448	-0.00544448
u^2		0.107422	0.142112	-0.00962904	0.00269565
u^3		-0.0363689	-0.0545066	0.00975125	-9.31427×10^{-4}
u^4		0.00772009	0.0145342	-0.00442079	0.00173662
u^5		-0.00126492	-0.00291698	0.00128249	-7.61018×10^{-4}
u^6		1.60790×10^{-4}	4.11474×10^{-4}	-2.40437×10^{-4}	1.54324×10^{-4}
u^7		-1.38523×10^{-5}	-3.69248×10^{-5}	2.69633×10^{-5}	-1.70449×10^{-5}
u^8		6.87170×10^{-7}	1.86585×10^{-6}	-1.61695×10^{-6}	9.99396×10^{-7}
u^9		-1.46371×10^{-8}	-4.02619×10^{-8}	4.00602×10^{-8}	-2.37364×10^{-8}

^{27}Al					
$u = p^2 b^2/2, b = 1.8405 \text{ fm}$					
$e^{-u} \times$	S_{00}	$S_{11} (1b+2b \text{ min})$	$S_{11} (1b+2b \text{ max})$	$S_{01} (1b+2b \text{ min})$	$S_{01} (1b+2b \text{ max})$
1	0.0888149	0.0256387	0.0412381	0.0949175	0.121145
u	-0.117822	-0.0539361	-0.0881079	-0.152223	-0.212484
u^2	0.0631336	0.0638570	0.0973265	0.108925	0.189337
u^3	-0.00919554	-0.0473962	-0.0555104	-0.0348055	-0.0898511
u^4	5.84421×10^{-4}	0.0242338	0.0200475	0.00826932	0.0309681
u^5	5.54484×10^{-4}	-0.00781004	-0.00447580	-0.00135106	-0.00679460
u^6	-1.15453×10^{-4}	0.00153205	6.45927×10^{-4}	1.93042×10^{-4}	0.00101787
u^7	1.40388×10^{-5}	-1.76118×10^{-4}	-5.82323×10^{-5}	-2.20321×10^{-5}	-9.71893×10^{-5}
u^8	-9.21830×10^{-7}	1.08574×10^{-5}	3.00602×10^{-6}	1.39046×10^{-6}	5.18194×10^{-6}
u^9	2.52336×10^{-8}	-2.75875×10^{-7}	-6.68767×10^{-8}	-3.63020×10^{-8}	-1.17607×10^{-7}
$e^{-u} \times$		$S_p (1b+2b \text{ min})$	$S_p (1b+2b \text{ max})$	$S_n (1b+2b \text{ min})$	$S_n (1b+2b \text{ max})$
1		0.209087	0.251154	0.00893959	0.0192751
u		-0.317485	-0.417183	0.00590871	-0.0132327
u^2		0.213007	0.344662	-0.0270773	-0.00545593
u^3		-0.0610495	-0.147056	0.0233435	0.0111533
u^4		0.0133827	0.0465970	-0.00948779	-0.00603345
u^5		-0.00157210	-0.00899070	0.00262032	0.00259059
u^6		1.66098×10^{-4}	0.00121558	-4.42643×10^{-4}	-6.07533×10^{-4}
u^7		-1.51579×10^{-5}	-1.05060×10^{-4}	4.79465×10^{-5}	8.40120×10^{-5}
u^8		8.74763×10^{-7}	5.13463×10^{-6}	-2.80932×10^{-6}	-5.86214×10^{-6}
u^9		-2.15130×10^{-8}	-1.07015×10^{-7}	6.92513×10^{-8}	1.64380×10^{-7}

TABLE VIII. Fits to the isoscalar/isovector structure factors S_{00} , S_{11} and S_{01} as well as “proton-only” and “neutron-only” structure factors S_p and S_n for spin-dependent WIMP elastic scattering off ^{29}Si , including 1b and 2b currents as in Fig. 13. The upper and lower limits from the theoretical error band were used for the fit. The fitting function of the dimensionless variable $u = p^2 b^2 / 2$ is $S_{ij}(u) = e^{-u} \sum_{n=0}^9 c_{ij,n} u^n$. The rows give the coefficients $c_{ij,n}$ of the u^n terms in the polynomial.

^{29}Si					
$u = p^2 b^2 / 2, b = 1.8575 \text{ fm}$					
$e^{-u} \times$	S_{00}	$S_{11} (1b+2b \text{ min})$	$S_{11} (1b+2b \text{ max})$	$S_{01} (1b+2b \text{ min})$	$S_{01} (1b+2b \text{ max})$
1	0.0140647	0.00434396	0.00692435	-0.0197473	-0.0155117
u	-0.0188522	-0.00978508	-0.0145952	0.0343683	0.0258450
u^2	0.0149891	0.0141312	0.0170700	-0.0349170	-0.0268086
u^3	-0.00542122	-0.0120045	-0.0101378	0.0178060	0.0173458
u^4	0.00117173	0.00602619	0.00368687	-0.00551301	-0.00805050
u^5	-1.15932×10^{-4}	-0.00177394	-7.87789×10^{-4}	8.86605×10^{-4}	0.00251057
u^6	2.47182×10^{-5}	3.11634×10^{-4}	1.05603×10^{-4}	-7.60246×10^{-5}	-5.25166×10^{-4}
u^7	-3.04480×10^{-6}	-3.20168×10^{-5}	-8.92530×10^{-6}	1.58691×10^{-6}	6.63557×10^{-5}
u^8	2.00549×10^{-7}	1.76286×10^{-6}	4.47332×10^{-7}	2.54524×10^{-7}	-4.41639×10^{-6}
u^9	-5.46011×10^{-9}	-3.97506×10^{-8}	-9.82815×10^{-9}	-1.38615×10^{-8}	1.19592×10^{-7}
$e^{-u} \times$		$S_p (1b+2b \text{ min})$	$S_p (1b+2b \text{ max})$	$S_n (1b+2b \text{ min})$	$S_n (1b+2b \text{ max})$
1		0.00125408	0.00296249	0.0337976	0.0409244
u		6.68801×10^{-4}	-0.00455830	-0.0515755	-0.0717867
u^2		-0.00210934	0.00942858	0.0452607	0.0799249
u^3		0.00149251	-0.0105616	-0.0201013	-0.0491256
u^4		-3.59430×10^{-4}	0.00655559	0.00538148	0.0197508
u^5		-4.73546×10^{-5}	-0.00221187	-7.60569×10^{-4}	-0.00486760
u^6		4.81182×10^{-5}	4.27089×10^{-4}	9.20786×10^{-5}	7.91536×10^{-4}
u^7		-9.10073×10^{-6}	-4.47737×10^{-5}	-9.01250×10^{-6}	-7.77097×10^{-5}
u^8		8.45631×10^{-7}	2.52194×10^{-6}	5.41575×10^{-7}	4.13236×10^{-6}
u^9		-3.00417×10^{-8}	-5.89991×10^{-8}	-1.39919×10^{-8}	-9.10412×10^{-8}